



university of  
 groningen

UNIVERSITY OF GRONINGEN

BACHELOR THESIS

---

# Constructing the frontend of the Kapteyn Interferometer and investigating the single dish configuration

---

*Author:*  
Mathijn LENSEN

*Supervisors:*  
Prof. Dr. Andrey BARYSHEV  
Dr. John P. MCKEAN  
Dr. Ronald HESPER

*Second examiner:*  
Dr. Ir. Willem JELLEMA

*A thesis submitted in fulfillment of the requirements  
for the degree of Bachelor  
in the*

Kapteyn Astronomical Institute

UNIVERSITY OF GRONINGEN

## *Abstract*

Faculty of Science & Engineering  
Kapteyn Astronomical Institute

Bachelor

### **Constructing the frontend of the Kapteyn Interferometer and investigating the single dish configuration**

by Mathijn LENSEN

In this Bachelor Thesis the frontend design of a simple, 2 element interferometer working at 11.2 GHz is discussed. The interferometric setup consists of two equatorial mounts, two offset paraboloidal dishes and 2 LNBs acting as receivers. Additionally, the single dish configuration is examined. The radiation pattern was determined showing clear side lobes at a level of approximately -17dB and the beam width was measured to be  $4.90^\circ$ . Furthermore, the illumination pattern is investigated to determine the optimal LNB placing. Using Y-factor calibration the receiver temperature was determined to be 110K up to 150K depending on the LNB placing. At last some sky measurements on an unstable sky were done resulting in atmospheric opacities at zenith of 0.039 and 0.053.

## *Acknowledgements*

At first I would like to thank my supervisors Andrey Baryshev, John McKean and Ronald Hesper for setting up this project and guiding me through the process. Working on the project for the last few months has been challenging and inspiring. The project has stimulated me to look further into the direction of engineering. The construction of certain parts during the process seemed difficult at first but after instructions from Ronald, Andrey Khudchenko and other [SRON](#) staff these things turned out to be quite easy. Finally I would like to thank my fellow students, Jasper Steringa and Casper Farret Jentink for their cooperation in this project. The mutual contribution and collaboration provided an advantage for all of us.

# Contents

<b>Abstract</b>	<b>i</b>
<b>Acknowledgements</b>	<b>ii</b>
<b>1 Introduction</b>	<b>1</b>
1.1 Radio astronomy and interferometry . . . . .	1
1.2 The Kapteyn Interferometer project . . . . .	2
1.3 Antenna temperature . . . . .	3
1.3.1 Brightness temperature . . . . .	3
1.3.2 Radiation pattern . . . . .	4
<b>2 Setup and operation</b>	<b>7</b>
2.1 The dishes . . . . .	7
2.2 The mounting . . . . .	11
2.3 The receiver . . . . .	13
<b>3 Noise, stability and calibration</b>	<b>16</b>
3.1 Noise . . . . .	16
3.2 Y-factor calibration . . . . .	17
3.3 Stability . . . . .	19
3.4 Sensitivity . . . . .	21
3.5 Allan variance . . . . .	22
<b>4 Radiation-and illumination pattern</b>	<b>26</b>
4.1 Radiation pattern . . . . .	26
4.1.1 Far field scan . . . . .	27
4.1.2 Near field scan . . . . .	32
Setup . . . . .	32
Results . . . . .	35
4.2 Illumination pattern . . . . .	39
4.3 Aperture efficiency . . . . .	43
<b>5 Elevation scan</b>	<b>45</b>
5.1 Determination of $\tau_0$ and $T_{rcv}$ . . . . .	45
<b>6 Conclusion and further research</b>	<b>49</b>
6.1 Conclusion . . . . .	49
6.2 Further research . . . . .	49
<b>A Python script for calibration and elevation scans</b>	<b>51</b>
<b>B Python script for determining Allan variance</b>	<b>53</b>
<b>C Python Script for determining beampattern using the FF-scan</b>	<b>55</b>

D Python Script for determining beampattern using the $NF_1$ -scan	57
Bibliography	65

# List of Abbreviations

<b>LNB</b>	<b>Low Noise Block Downconverter</b>
<b>VNA</b>	<b>Vector Network Analyser</b>
<b>RMS</b>	<b>Root Mean Square</b>
<b>OPD</b>	<b>Optical Path Difference</b>
<b>RF</b>	<b>Radio Frequency</b>
<b>IF</b>	<b>Intermediate Frequency</b>
<b>LO</b>	<b>Local Oscillator</b>
<b>NF<sub>1</sub></b>	<b>Near Field</b>
<b>FF</b>	<b>Far Field</b>
<b>FWHM</b>	<b>Full Width Half Maximum</b>
<b>HFBW</b>	<b>Half Power Beam Width</b>
<b>NF<sub>2</sub></b>	<b>Noise Figure</b>
<b>CMB</b>	<b>Cosmic Microwave Background</b>
<b>LFB</b>	<b>Low Frequency Band</b>
<b>HFB</b>	<b>High Frequency Band</b>
<b>ALMA</b>	<b>Atacama Large Millimeter Array</b>
<b>SKA</b>	<b>Square Kilometer Array</b>
<b>WSRT</b>	<b>Westerbork Synthesis Radio Telescope</b>

## Chapter 1

# Introduction

### 1.1 Radio astronomy and interferometry

In the 1860's, James Clerk Maxwell showed us that electromagnetic radiation comes from electricity and magnetism and can be found at any wavelength. The field of radio astronomy spans the electromagnetic window from approximately 30 MHz (10m) up to 700 GHz (0.4mm). In the 1930's Karl Jansky was the first one to detect radio waves coming from an astronomical source. Using an array of large directional antennas he detected a repeating radio signal, which he eventually concluded to come from the galactic centre (1933). The era of radio astronomy in the Netherlands started on 15 April 1944, when Hendrik Christoffel (Henk) van de Hulst predicted that the neutral hydrogen spectral line should be detectable in the radio-window (Woerden and Strom, 2006), now known as the 21 cm line. After World War II, Van de Hulst's phd-supervisor, Jan Hendrik Oort became director of the observatory in Leiden and took the lead in Dutch radio astronomy. With his help, in 1956, The Dwingeloo Radio telescope was put into operation to investigate the centre of the Milkyway. Fourteen years later, again under effort of Oort, the Westerbork Synthesis Radio Telescope (WSRT) was built. The WSRT is an aperture synthesis interferometer, meaning it combines the signals of multiple telescopes providing higher angular resolution by the means of interferometry. Nowadays, radio astronomy and interferometry are practically fused together which have resulted in incredible projects such as the Atacama Large Millimeter Array (ALMA) and the upcoming Square Kilometre Array (SKA).

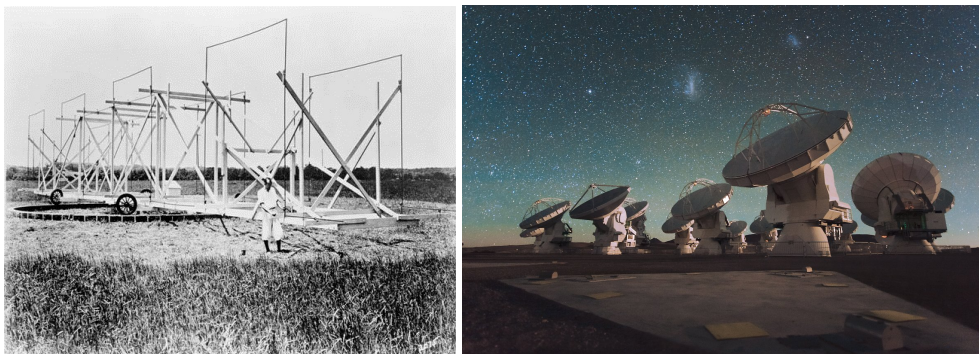


FIGURE 1.1: Left: Jansky and his array of antennas. Right: The Atacama Large Millimeter Array

## 1.2 The Kapteyn Interferometer project

The purpose of this bachelor thesis is to describe the process of constructing a simple, two element interferometer and to investigate various properties of the single dish configuration and their interpretation. The final goal of the collaborative project is to determine the angular size of the sun. To get to this goal there are certain steps to be taken. These steps have been divided among three students and are represented in their respective bachelor theses. The parts are divided in such a way that each one focuses on a different aspect and has an equal workload.

One project is to simulate visibilities or the response of the interferometer for different objects. This part is done by Jasper Steringa (Steringa, 2018), using his findings the output-data of the interferometer can be compared to the theoretical expectation.

The second part is done by Casper Farret Jentink (Farret Jentink, 2018). His project concerns the back-end of the interferometer and the interpretation of the data. At the end his findings will give an estimate of the angular size of the sun.

My part in this project mainly concerns single dish operation and the front-end construction of the interferometer. For the single dish this means determining certain valuable parameters such as the receiver temperature and mapping the radiation-pattern. For the interferometry part this includes finding out which dishes and mounts are suitable for our project and cooperating them into the setup. Finally some tests on the stability of the system and some sky measurements were done to determine the atmospheric opacity and system temperature. For all the single dish measurements, the same dish was used every time which is assumed to give the same results as for the other dish.

Furthermore, in this thesis there is sometimes referred to the Kapteyn Radio Telescope or KRT, a horn-telescope made by fellow-students in 2015. The project which they did is similar to ours hence some comparisons can be found in this thesis.

All the computational work was done in [Python](#) and all errors in this thesis were calculated using the [Astropy](#) module.

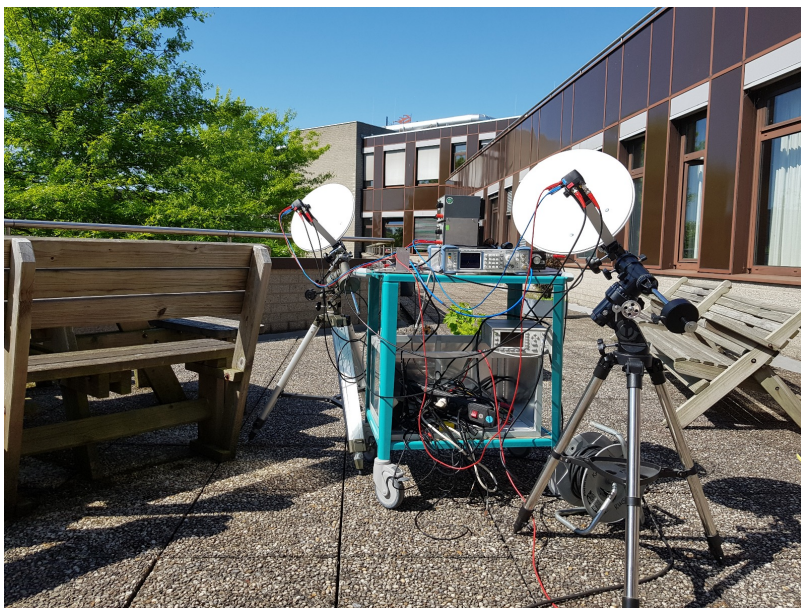


FIGURE 1.2: The interferometer, KISS (Kapteyn Interferometer for Short-baseline Solar observations.)



### 1.3 Antenna temperature

To do accurate, calibrated measurements of astronomical sources, the power response of an antenna system is the most important characteristic to know. The output power per unit bandwidth  $P_\nu$  for an antenna is described by

$$P_\nu = \frac{1}{2} A_e \iint B_\nu(\theta, \phi) P_n(\theta, \phi) d\Omega. \quad (1.1)$$

In this equation  $B_\nu(\theta, \phi)$  is the brightness distribution and  $P_n(\theta, \phi)$  is the normalized power pattern. Furthermore  $A_e$  is the effective area and  $d\Omega$  is the beam solid angle.

Using the Nyquist theorem, described in section 3.1 this can be translated to an equivalent antenna temperature given by

$$T_{ant} = \frac{1}{2k} A_e \iint B_\nu(\theta, \phi) P_n(\theta, \phi) d\Omega, \quad (1.2)$$

where  $k$  is the Boltzmann constant.

#### 1.3.1 Brightness temperature

The brightness distribution describes the brightness profile coming from sources in direction on which the antenna is pointed at. It is commonly described by the brightness temperature of a black body. A black body is an opaque and non-reflective body which absorbs all incoming electromagnetic radiation before emitting it again. The emitted radiation has a specific (Planck) spectrum with the intensity only dependent on the thermodynamic temperature of the body (Loudon, 2000). For the measurements done in this project, all objects are approximated as being a black body for the sake of simplicity, which is usually a plausible assumption. The brightness spectrum of the emitted electromagnetic waves from a black body is given by Planck's law (Fig. 1.3),

$$B_\nu(T) = \frac{2h\nu^3}{c^2} \frac{1}{e^{\frac{h\nu}{kT}} - 1}, \quad (1.3)$$

where  $h$  is Planck's constant,  $c$  is the speed of light,  $\nu$  is the specific frequency and  $T$  the thermodynamic temperature of the body.

Most of the objects in daily life have a temperature of approximately room temperature ( $\approx 295\text{K}$ ) corresponding to most of the radiation being emitted in the infrared. For the sun, the temperature is much higher ( $\approx 5800\text{K}$ ) so that most of the radiation is emitted at wavelengths visible to the human eye.

At radio frequencies/wavelengths, Planck's law can often be approximated by the Rayleigh-Jeans Law given by

$$B_\nu(T) = \frac{2\nu^2 kT}{c^2}, \quad (1.4)$$

with the condition that  $h\nu \ll kT$ . In Figure 1.3 the Rayleigh-Jeans curve is represented as the classical theory.

Since the spectral brightness  $B_\nu$  and the temperature  $T$  are proportional, the brightness can be measured in values of  $T$  so that we find

$$T_b = \frac{c^2}{2k\nu^2} I_\nu, \quad (1.5)$$

where  $T_b$  is the brightness temperature of the source and  $I_\nu$  is the spectral intensity.

In this thesis  $T_{ant}$  is mostly substituted for  $T_b$  being a description of the brightness of a source, rather than the physical thermodynamic temperature.

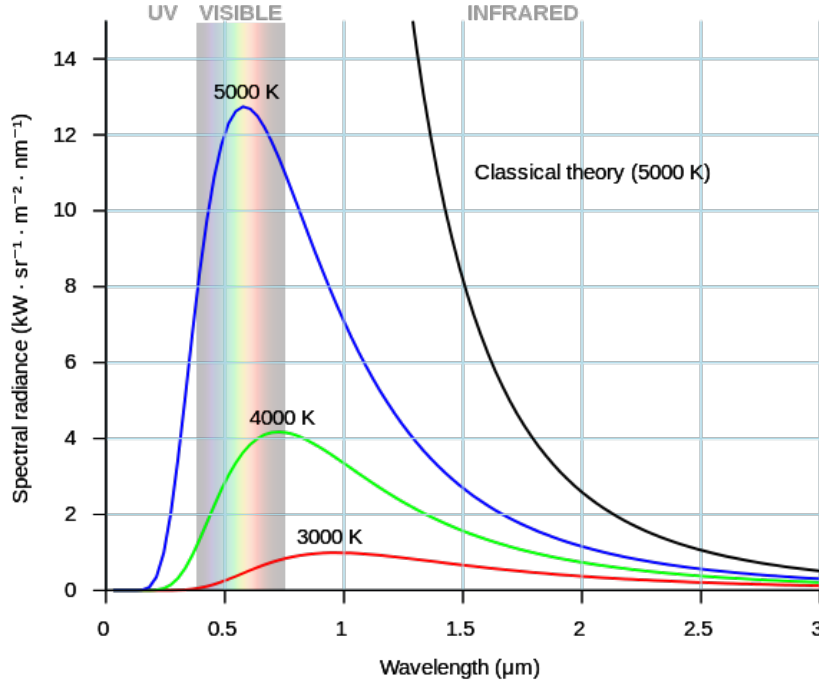


FIGURE 1.3: Figure showing the Planck curves for different thermodynamic temperatures and the comparison with the classical Rayleigh-Jeans model. Image source: [wikipedia](https://en.wikipedia.org/wiki/File:Planck_radiation_5000K.jpg)

### 1.3.2 Radiation pattern

The antenna temperature does not only depend on the brightness temperature of observed source(s) but also on the (normalized) power pattern  $P(\theta, \phi)$ .

The power pattern is often named the (far field) radiation pattern. This radiation pattern describes the directional (angular) dependence of the strength of the radio waves from the antenna or other source (Balanis, 1982). To interpret the radiation pattern of an antenna, a diagram is often used. Since the radiation pattern is angular dependent, it is mostly shown as a polar diagram as can be seen in Fig. 1.4.

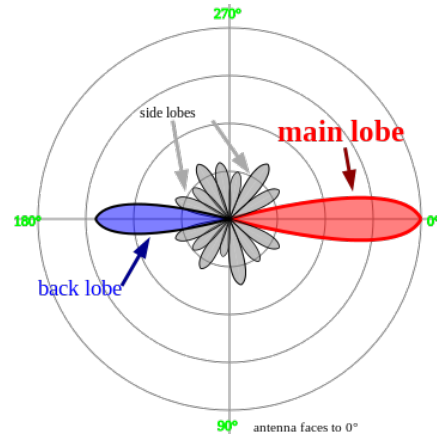


FIGURE 1.4: Standard radiation pattern for a dish antenna showing the main lobe, back lobe and side lobes in a polar representation. Image source: [wikipedia](#)

One can clearly see that the pattern consists of multiple lobes and is not isotropically responsive. The main lobe is mostly used to observe a source while the side lobes and back lobe (caused by interference) are ought to be minimized. The power response is described as the gain or directivity of the antenna mostly given in decibels (dB). The relative power can be calculated in dB using

$$L = 10 \cdot \log\left(\frac{P_1}{P_0}\right), \quad (1.6)$$

where  $P_1$  is the measured power and  $P_0$  is the reference power.

A rectangular radiation pattern in dB scale can be found in Fig. 1.5 and a 3D representation in Fig. 1.6.

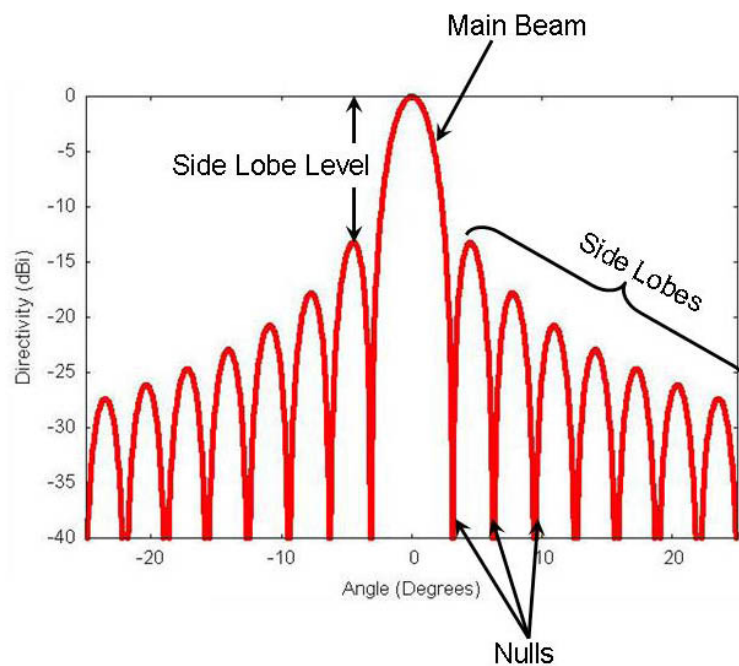


FIGURE 1.5: Typical radiation pattern on rectangular plot where the maximum is normalized to 0 dB. Image source: [wikipedia](#)

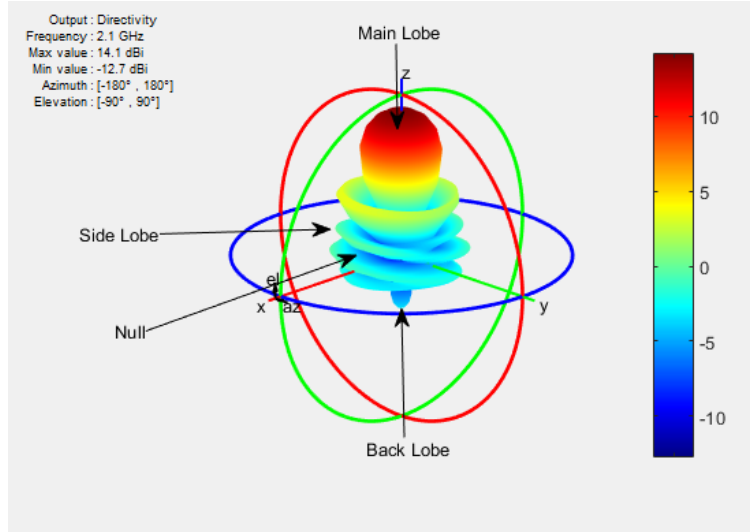


FIGURE 1.6: 3-dimensional representation of the radiation pattern of a certain antenna. Image source: [mathworks](#)

To characterize the spread of the main lobe or the beam width of the antenna the Half Power Beam Width or Full Width Half Maximum is used. This is the angle between the points where the main lobe has decreased to half of the maximum. In dB scale this corresponds to a drop of -3 dB.

For parabolic antennas the FWHM or beam width is given by

$$\theta_{bw} = K \frac{\lambda}{D}, \quad (1.7)$$

where  $\lambda$  is the observing wavelength,  $D$  is the diameter of the dish and  $K$  is a factor depending on the shape of the dish and its illumination. For an ideal uniformly illuminated parabolic reflector and  $\theta$  in degrees,  $K$  would be 57.3. For a "typical" parabolic antenna  $K$  would be approximately 70 (Minoli, 2009).

A fundamental property of an antenna is that the radiation pattern when the antenna is used for receiving is identical to if it were transmitting as a consequence of [reciprocity](#). This property will be exploited in this thesis to make things easier.

The radiation pattern of an antenna can be determined experimentally using a near field scanner or by doing a far field scan, both methods will be used in this project.

## Chapter 2

# Setup and operation

### 2.1 The dishes

At the beginning of the project the choice had to be made which antenna type and frequency band was to be used for the interferometric setup. We chose to set our observing frequency in the ballpark of approximately 11 GHz. Since the radio waves at this frequency have a small wavelength they can be used for point-to-point communication. The narrow beams can be directed from aperture antennas such as horn or parabolic antennas without interfering with nearby transmitters on the same frequency. For this reason it is mainly used for the transmission of satellite television. Due to this enormous economical advantage, this was also used as the frequency for our experiment. This would imply working in the X or  $K_u$  frequency band. The X band ranges from 8.0 to 12.0 GHz where the  $K_u$  band ranges from 12.0 to 18.0 GHz. (IEEE, 2003).

One possibility could be to use two identical horn-antennas. There are different horn-types which could have been used such as the Picket-Potter horn constructed by Lap et al, (Lap, 2015). It was decided that these horns would have cost a lot of time to construct compared with the other possibilities. The paraboloidal antenna, a dish reflector with a cross-sectional shape of a parabola was the second option. The advantage of a parabolic dish is that it has a high directivity compared with a horn. A high directivity translates to a narrow beam so that sources from a particular direction can be distinguished. Moreover, dish antennas are widely available on the commercial market making it a superior alternative to buy one compared to making one ourselves. Paraboloidal antennas can be distinguished by shape such as cylindrical or 'shaped-beam' antennas. Furthermore different types are classified by the type of feed they have. The antenna feed is the component which feeds the radio-waves to the rest of the antenna structure. Various feeds such as axial, off axis or Gregorian can be used with each their advantages. The off-axis dish was the most interesting. The advantage of this configuration is that there is (almost) no obstruction of the beam by the antenna feed, i.e. it has a relatively high aperture efficiency. This means that the dish can be smaller compared with other configurations which have a lower aperture efficiency (but the same forward gain) providing higher mobility. This is the main reason that it is widely used in satellite television.

For our experiment a certain sensitivity is needed to distinguish the sun's signal from noise, implying that a certain forward gain or aperture is necessary. It was calculated (3.4) that the aperture is of least concern so that the smallest dishes available possible is the way to go. We chose to go with the 35cm 'campingschotel in koffer' from Astrasat. The dishes come with a quite clever attachment so that they can be easily mounted to certain surfaces. A nice case is also provided so that the mounts

are quite mobile and can be set up fairly quickly. There was no list of specifications included and no information was made public on the internet so some things had to be measured at first. The dimensions of the dish were accurately measured which can be found in Table 2.1.

TABLE 2.1: Measured specifications of the dish

Parameter	Value
Semi minor axis length $D$	$352 \pm 3$ mm
Semi major axis length $L$	$402 \pm 3$ mm
Maximum depth $B$	$37.2 \pm 0.3$ mm

The geometry of an offset parabola can be seen in Fig.2.2. Since the height and width of the dish are unequal, it is not radially symmetric but the rim traces out an ellipsoid. The projection onto the  $x,y$ -plane on the contrary is circular, implying that the reflector surface is paraboloidal with an eccentricity of 1. The spherical projection onto the  $x,y$ -plane of an ellipsoid means that the dish has to be tilted a certain angle. This angle is called the elevation angle  $\phi$ , the angle on which the beam is projected on the sky when the dish is leveled with the ground surface as can be seen in Fig.2.1. The elevation angle can simply be calculated using

$$\phi = \arccos\left(\frac{D}{L}\right). \quad (2.1)$$

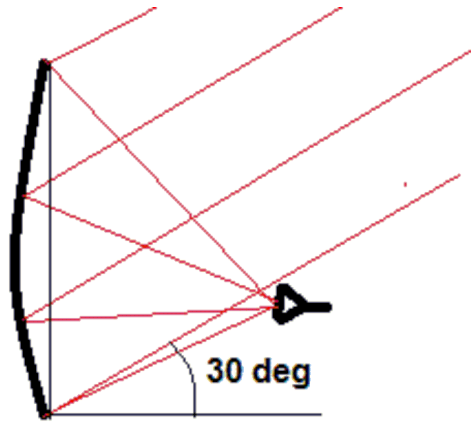


FIGURE 2.1: Parabolic dish with a 30 degree offset design, when the front of the dish is vertical, the beam elevation is 30 degree. Image source: [Satsig](#)

The focal length  $F$  can be calculated with

$$F = \frac{D^3}{16LB} \quad (2.2)$$

as derived by Uhm and Park (M. Uhm and Park, 1996).

The focal point is the point where the LNB should be placed so that the highest power is measured. The LNB should be placed exactly at a distance  $F$  from the bottom-rim of the dish for optimal results (Rensburg, 2012).



Another contributing element are the shape errors, random surface errors in the dish reducing the efficiency. An approximation of the shape errors is the Ruze equation,

$$\eta = \exp - \left( \frac{4\pi\epsilon}{\lambda} \right)^2, \quad (2.6)$$

where  $\epsilon$  is the RMS of the surface deviations.

The RMS and so the reflective efficiency of our dish will be determined using the phase measurements of the aperture in section 4.3.

Another factor is feed spillover, part of the beam of the LNB misses the reflector, resulting in less power from the source reaching the feed. It also has to be taken into account that the part missing the reflector can add a substantial power to the total, in the case that the surroundings are relatively hot.

The Taper efficiency is another influence, the distribution of power-response over the antenna aperture. The power response of the feed antenna usually diminishes towards the rim of the dish, creating an uneven illumination and so lowering the efficiency and gain. Increasing the F/D ratio will increase the taper efficiency, however this will increase feed spillover.

Moreover, the radiation pattern contains side lobes and a back lobe, probably adding power from the surroundings. In section 4.2 and 4.1 the illumination and radiation pattern will be discussed thoroughly.

Other factors contributing to the aperture efficiency can be losses in the feed, defocusing, cross polarization or antenna feed mismatch. For reflector antenna's the aperture efficiency ranges from 50 to 80 percent (Lehpamer, 2010). An aperture efficiency of 60-70 percent is estimated for our system. The dish is of low quality with palpable height differences and protruding bolts on the effective area, implying low reflective efficiency.

Theoretically the beam width of our dish would be  $0.0760K$  with  $K$  the shape factor according to Eq. 1.7. If the dish were evenly illuminated, this would correspond to a beam width of  $4.33^\circ$  while the expected (gaussian) beam width is  $5.29^\circ$ . The k-factor will be determined in section 4.1.1.

TABLE 2.2: Calculated specifications of the dish

Parameter	Value
focal length $F$	$182 \pm 4 \text{ mm}$
elevation offset angle $\phi$	$28.9 \pm 0.2^\circ$
F/D ratio	$0.52 \pm 0.02$
Geometric area $A_{geo}$	$0.445 \pm 0.006 \text{ m}^2$
Projected geometric area $A_{pgeo}$	$0.389 \pm 0.005 \text{ m}^2$
Directivity $\mathcal{D}$ or Gain $G_{max}$	$1704 \pm 6$ or $32.3 \text{ dBi}$



## 2.2 The mounting

An important part of the interferometer is the mounting. The mounts should fit our project by means of characteristics. The mounts should be stable enough so that wind and ground vibrations are negligible. At last the total setup should be made in a way that it can be used from the balcony of the Kapteyn institute which is either convenient for this project as for future research. There are a few options which would suit these conditions. At first, mounts in the form of clamps could be used to mount the two dishes to the balustrade of the Kapteyn Institute balcony. This would be a low-cost and easy way of mounting which also results in a sturdy alt-azimuth configuration. The dish can be moved around using a ball-head so that it can be moved in any direction. The disadvantage of this mounting is that you are bound to choose a certain orientation according to an object on the sky and that the baseline is limited to a certain length. Furthermore it is hard to orient both dishes in exactly the same way so that both beams are parallel.

The second and third option are mobile stand-alone alt-azimuth mounts or Equatorial mounts. Alt/az-mounts are simple two-axis mounts which can move the dish in horizontal or vertical direction. The simple configuration makes it stable and cheap which is the reason it is mainly used for large professional (radio)telescopes such as ALMA and the Very Large array (VLA). When doing drift-scans these mounts will not be a problem because the mount should be locked in a certain position. Also for tip-scans, this mount is fine because one only has to move the orientation of the dish in vertical direction (altitude). When you would like to see how the response of an object changes as a function of time, tracking is necessary. The disadvantage of this mount is that it requires two axis rotation to track an object on the sky. The solution to this problem is the last option, an equatorial/parallactic mount. An equatorial mount has one axis parallel to the axis of rotation/directed to the celestial pole by which it compensates for the earth's rotation. This ensures that only one axis has to be moved at constant speed to stay fixed at any celestial object with diurnal motion. The advantage of only having to move one axis to track an object decreases the offset-errors in the obtained data.

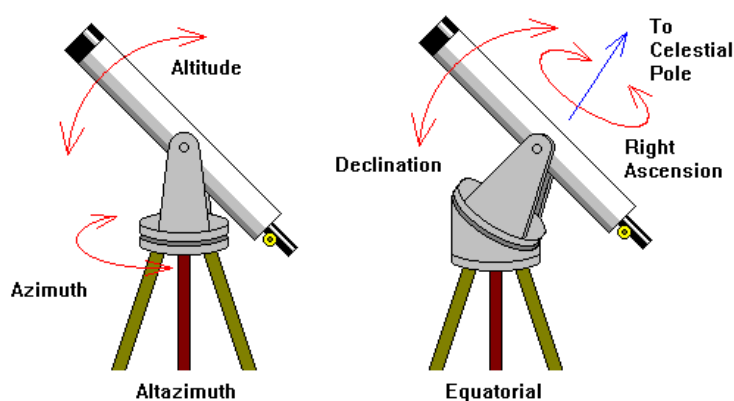


FIGURE 2.3: Diagram visualising the working of an Alt/az and Equatorial mount. Image source: [Science at your doorstep](#)

Two, simple, equatorial mounts without tracking were already available to be borrowed when the project started. The mounts had different dimensions but they could be made to work together to make a temporary setup. Some machining had to be done so that both dishes could be mounted to the mounts. Using drills and

milling machines one plastic attachment was made which could fit the dovetail-clamp of the mount perfectly (see Fig. 2.4). For the other mounts a piece of aluminum was processed so that the dish could be mounted sturdy to the mount. This setup was used for a number of measurements before other mounts were bought. Two 'Skywatcher' EQ-1 mounts were bought to have a permanent setup. Additionally two electronic motor drives were bought to make tracking available. Using the new mounts with tracking, objects such as the Sun could be studied more easily. Furthermore different aspects of these objects have been made available for examination due to the tracking feature.



FIGURE 2.4: Mounting of the dishes to the mounts for the temporary setup.

For the new mounts, some adjustments had to be made. The new mounts had a very clumsy attachments so that something had to be figured out for the setup to work. Using some more machining, two aluminum blocks were produced so that they can be screwed onto the mounts and the dishes could be mounted on top. The tracking devices were assembled and connected to the mounts as can be seen in Fig. 2.5.



FIGURE 2.5: Mounting of the dishes to the mounts for the permanent setup with on the bottom, the tracking devices.

## 2.3 The receiver

The receiving device in our case is a heterodyne system: a LNB or Low-Noise Block down converter. It works in following way: microwave radiation is picked up by the feedhorn and supplied to a small pin (the antenna) through a section of waveguide. Most LNB's have 2 pins at right angles so that different polarization's can also be received. The electric signal is directed to a circuit board for further processing. The circuit board consists of a low noise amplifier, frequency mixer, local oscillator and intermediate frequency (IF) amplifier through which the signal is directed. The frequency block (RF) is down converted to a lower IF so that the signal can be transmitted via relatively cheap coaxial cables. The cross-section of a LNB can be seen in Fig. 2.7, showing all the components. Finally, the down converted signal is read out by a power-meter. A more detailed description of the LNB functioning has been done by Farret Jentink (Farret Jentink, 2018).

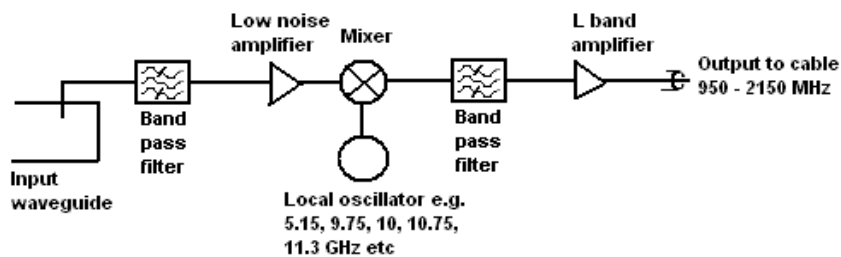


FIGURE 2.6: Diagram showing the principle of an LNB. Image source: [Satsig](#)

The output from the power-meter can be read of the LCD screen. Using a [Raspberry pi](#) the output of the power-meter can be saved on it's internal server and can be moved to your own computer. In our case we chose to go with an X-band LNB because this was the most convenient choice. These LNB's are widely sold and are relatively inexpensive. The [EVO single LNB](#) also bought at [Astrasat](#) turned out to be our best choice since it has a low noise figure (NF) and high frequency stability. Besides it has the feature to receive horizontal and vertical polarization. The exact specifications of the LNB can be found in table 2.3

TABLE 2.3: Specifications of the EVO single LNB

Parameter	Value
Input frequency range: Low Band	10.7 - 11.7 GHz
Input frequency range: High Band	11.7 - 12.75 GHz
Gain (typical)	60 dB
Noise Figure NF (typical)	0.1 dB
L.O. Frequency	9.75 GHz
Output frequency: Low band	950 - 1950 MHz

The input frequency of the Low Band was set as our standard. The observing frequency  $\nu$  was set to 11.2 GHz with a bandwidth  $\Delta\nu$  of 1 GHz and all measurements will be done in this band. For the measurements done by Farret Jentink, (Farret Jentink, 2018) an additional filter with a bandwidth of 40 MHz was used, reducing the span of the observing frequency. The gain of the system is the total amplification from the received signal up to the signal read out by the power meter. The LNB is stated to have a  $NF_2$  of 0.1 dB in typical circumstances which would imply a receiver temperature  $T_{rcv}$  of approximately 7K through

$$F = 10^{\frac{NF}{10}} = \frac{SNR_{in}}{SNR_{out}} = 1 + \frac{T_{rcv}}{T_0}, \quad (2.7)$$

where  $F$  is the noise factor, SNR is the signal to noise ratio and  $T_0$  the standard noise temperature ( $\sim 295K$  at room temperature).

The validity of the 'typical' receiver temperature stated by the manufacturer will be tested in section 3.2.

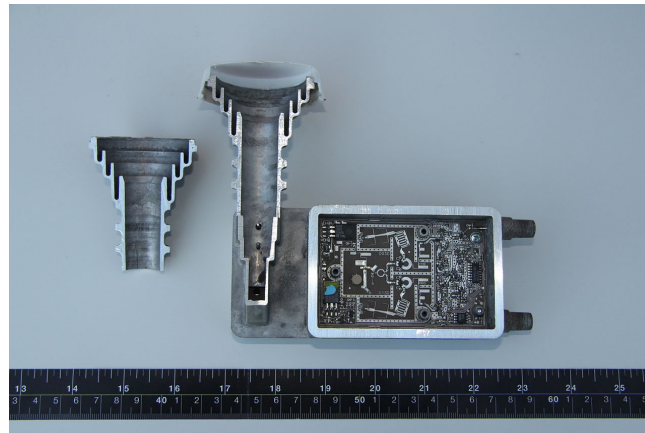


FIGURE 2.7: An LNB cut in half showing the small horn, waveguide, antenna pin, circuit board on the coaxial output. Image source: [wikipedia](#)

For the LNB's to fit our project, they had to be adjusted. The LNB's had to be phase-locked to preserve the phase-information in the obtained data. This was done by removing the crystal of the oscillator and coupling both LNB's to an external function generator as reference . Originally the power for the LNB was supplied via the coaxial cable, these 2 signals had to be separated so that the LNB finally had 4 ports; 2 for the power (@ 13 Volt/ 110 mA), 1 for the external reference (@ 25 MHz/ -2dB) and 1 for the power output.



## Chapter 3

# Noise, stability and calibration

### 3.1 Noise

When using a measurement system, the ideal case would be that the measured output would only come from the source of interest. In reality this is never the case. In electronic systems there always is an unwanted random disturbance in your signal which we call noise. For our system, electromagnetic radiation is received by the LNB and goes through a lot of components before being read out by the power-meter. In this system, various noise types are present with presumably the most prominent one being thermal noise. Thermal or Johnson–Nyquist noise is generated by thermally agitated charge carriers inside an electrical conductor which is independent of applied voltage. The total noise present in the output signal can be described as the receiver noise or its corresponding receiver temperature using

$$P_v = kT. \quad (3.1)$$

The total output or system temperature of our measurement system will then be equal to receiver temperature plus the signal received from external sources:

$$T_{sys} = T_{ant} + T_{rcv}, \quad (3.2)$$

where  $T_{ant}$  is the antenna temperature of the external sources and  $T_{rcv}$  is the internal receiver temperature.

Not only the noise of the components in our system is incorporated into this equation.  $T_{ant}$  consists, next to the source of interest also of other external influences such as radiation emitted by the atmosphere, ground, surrounding buildings or the CMB. Summing up all these contributions, Eq.3.2 can also be written as

$$T_{sys} = T_{source} + T_{sky} + T_{ground} + T_{spill} + T_{CMB} + T_{rcv}. \quad (3.3)$$

All these separate terms contribute to the total system temperature.  $T_{sky}$  is the contribution of radiation coming from the atmosphere or sky.  $T_{ground}$  is the radiation coming from the ground which is captured by the dish in either the main lobe or side lobes of the beam.  $T_{spill}$  is the part of the feed antenna which misses the reflector dish, spillover.  $T_{CMB}$  is a 'constant' term with a current value of 2.73K originating from the big bang. As already stated before, the receiver temperature is an internal parameter and can be determined experimentally by calibrating the system. The calibration will be described in section 3.2.

In instrumentation and electronics, one of the most important properties of a measurement system is its linearity. Linearity is necessary to calibrate a system so that the obtained data can be interpreted. Linearity means that when measuring an dependent variable, the measured output should be directly proportional to an

independent variable, e.g. the output is directly proportional to the input. In reality, a measurement system can never be completely linear, most equipment is desired to have a certain degree of linearity in a specific range and will be non-linear outside of this range. In our case, linearity plays a role concerning the amplifiers within the LNB. In Figure 3.1 one can see the output of an amplifier plotted against the input where the ratio between the output and the input is defined as the gain. One can clearly see that there is a linear relation so that gain is constant, but at a certain point it starts to change. At the region far below the 1 dB compression point, where the gain deviates from the ideal gain with 1 dB, the system is said to be linear. The gain of a system can be determined using calibration as described in section 3.2

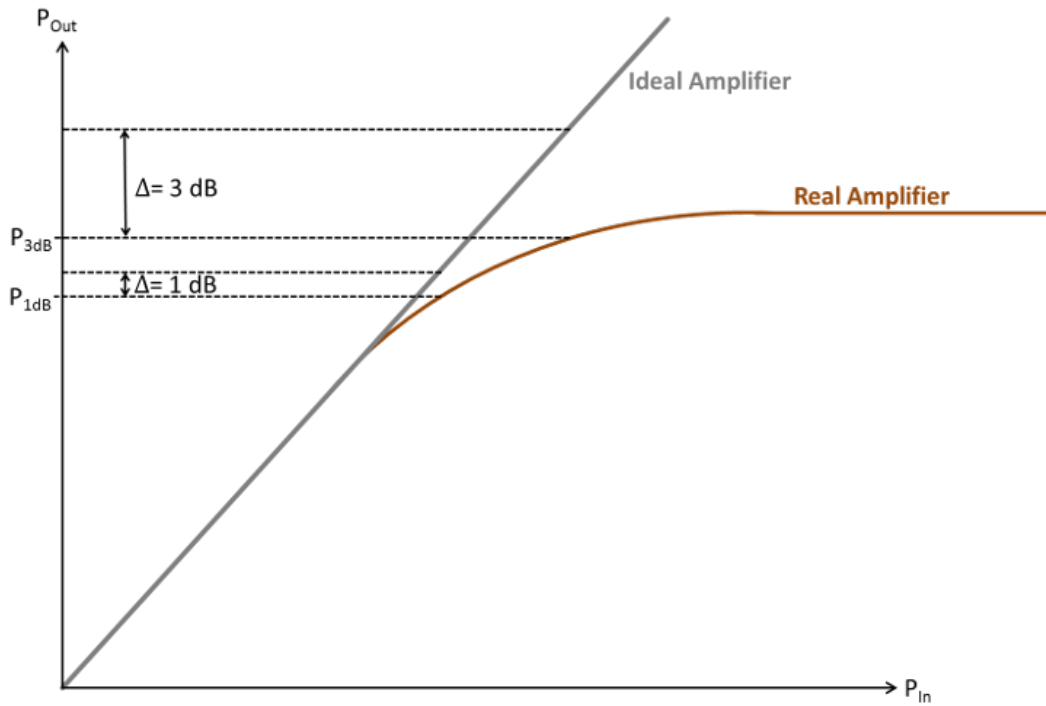


FIGURE 3.1: Figure showing the response of the output as function of input for an (ideal) amplifier. Image source: [SHF communication technologies](#)

## 3.2 Y-factor calibration

To interpret the data obtained by the measuring device, in our case a heterodyne receiver system, calibration is necessary. By comparing measured values with the known corresponding standard, a calibrated device can be achieved. For our project we will calibrate the telescope using the Y-factor calibration method (Wilson, Rohlf, and Hüttemeister, 2013). By defining the hot load to be a black body emitter at a certain known thermodynamic temperature and the cold load to be another black body emitter at a lower, known thermodynamic temperature, the 2 main ingredients are obtained. The output of the measurement system for the hot and cold load can be related to the known temperature using the system gain  $G$  of the system,

$$z_{cold} = (T_{cold} + T_{rcv})G \quad (3.4)$$

$$z_{hot} = (T_{hot} + T_{rcv})G. \quad (3.5)$$

Using these equations it follows that the receiver temperature  $T_{rcv}$  can be determined by

$$T_{rcv} = \frac{T_{hot} - T_{cold}Y}{Y - 1} \quad (3.6)$$

where  $Y$  is defined as

$$Y = \frac{Z_{hot}}{Z_{cold}}. \quad (3.7)$$

In our project most powers will be measured in dBm. dBm is a power measure in dB measured with respect to a reference of 1 mW which makes it an absolute measure of power. The power can be converted to mW by

$$P[mW] = 1mW \cdot 10^{P[dBm]/10}. \quad (3.8)$$

Furthermore the output of the power-meter can be related to the system temperature using

$$P[mW] = T_{sys} k_b \Delta\nu G. \quad (3.9)$$

Finally, the gain of the system can be determined with

$$G = \frac{P_{hot} - P_{cold}}{k_b \Delta\nu (T_{hot} - T_{cold})}. \quad (3.10)$$

Now using the output power and equation 3.6, the receiver temperature can be determined. Now the system is calibrated and can be used to determine brightness temperatures of certain phenomena. Note that it is important to keep the calibration up to date. The system should be calibrated just before the measurement and preferably between every measurement when doing tip scans so that the receiver information is up to date. A well calibrated system will ensure consistency of the measurements and so the interpreted data to be correct.

Using the calibration procedure explained above, the receiver temperature and gain of solely the LNB and LNB + dish were determined. In Figure 3.2 the measurement to determine the powers of the hot and cold load can be seen. For the part between 35 and 45 seconds, the LNB was pointing at the cold load (liquid nitrogen), corresponding to 0.0063 mW and 77.15 K for  $P_{LNB,cold}$  and  $T_{cold}$  respectively. The part between 200 and 300 seconds corresponds to  $P_{LNB,hot}$  and  $T_{hot}$  with 0.0135 mW and 295.25 K respectively. The part between 360 and 420 seconds corresponds to  $P_{dish,cold}$  with 0.0074 mW and the part from 550 to 570 seconds matches  $P_{dish,hot}$  with 0.0132 mW. The temperatures of the hot and cold load are the same for both setups. For all power measurements of the cold load, the minimum power was taken because this would correspond to (hopefully) all of the beam being filled. Furthermore, all the values below -22 dBm are due to the connectors making bad contact and are neglected.



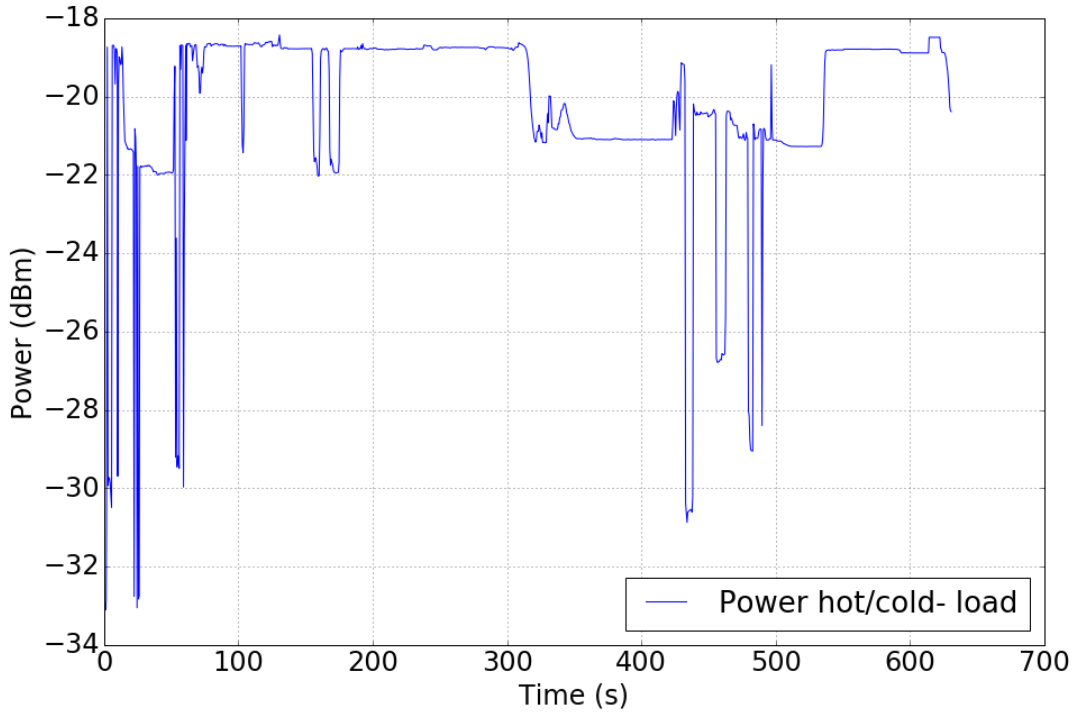


FIGURE 3.2: Measurement of the power of the hold and cold load for the setup with LNB only and the setup with LNB + dish.

Using Eq. 3.10 the gain of the LNB + dish was found to be 76 dB. Additionally  $T_{rcv,LNB}$  was found to be 113K while  $T_{rcv,dish}$  is equal to 208K. Theoretically, these system temperatures should be the same unless there is spillover. Another obvious reason could be that the cold load was not big enough to fill the whole beam. The spillover of the system is more accurately described in section 4.2. Using Eq. 2.7 and the calculated receiver temperature, the  $NF_2$  of the LNB was found to be 1.4 dB. This is far from the 0.1 dB specified by the manufacturer which could be explained by not having ideal conditions.

### 3.3 Stability

On the 17th and 18th of may 2018 the stability of a (single dish) system was determined. Using the hot load as calibrator, long time measurements were done where the beam of the dish was completely filled by the calibrator acting as a black body radiator (Fig. 3.3). The measurement was done with the phase locked system and the output of the measurements can be seen in Fig.3.4.



FIGURE 3.3: The setup used for the stability measurements. The beam is completely filled by the blue material, a RF absorber acting as a black body.

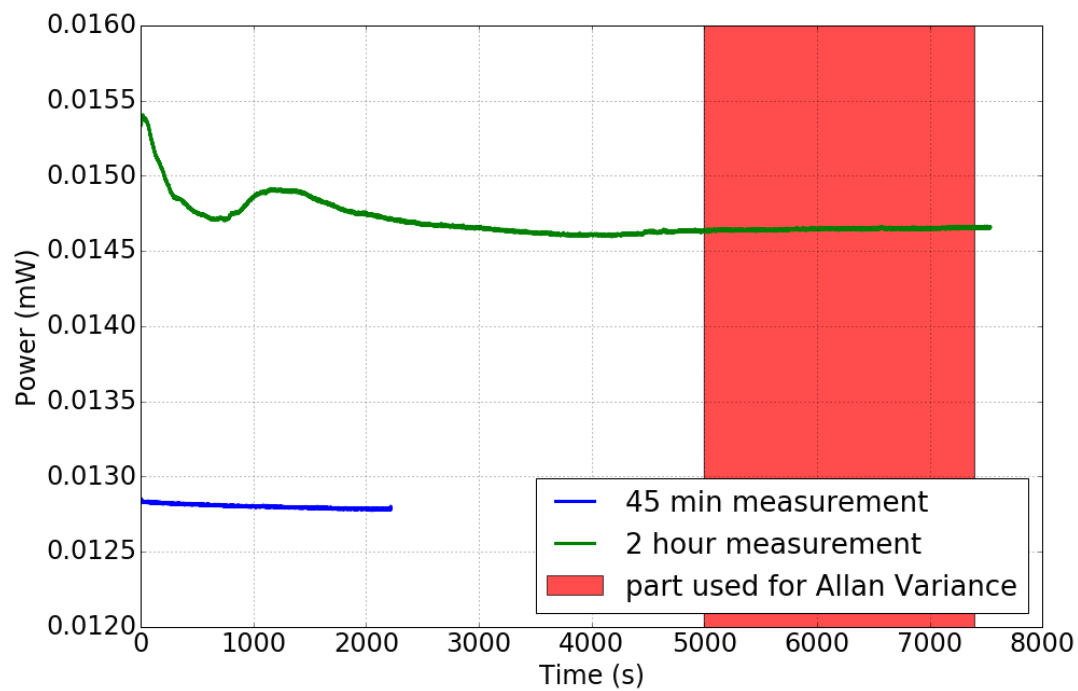


FIGURE 3.4: Figure showing the power response of the stability test for the hot load (a calibrator at room temperature, approximately 295K.) The red block represents which part of the 2 hour measurement is taken into account to calculate the Allan variance.

For the stability tests of the hot load, only the ambient temperature plays a role. Keeping the room temperature constant, the fluctuations of the hot load can be determined. In Fig. 3.4 it is visible that for the 2 hour measurement, the power drops approximately 5 percent in the first 600 seconds. This behaviour was seen in all the measurements so far. An explanation could be that the door to the room was suddenly closed for a long time so that the room could stabilize at a temperature lower than on the hallway, causing a drop in temperature. Furthermore a peak at approximately 1100s can be seen, the reason for this is that someone opened the door of the room and hot air started flowing inside.

For the Allan variance plot, only the part from 5000 to 7300 s was taken into account because the ambient temperature was most stable in this region. For the part from 5000 to 7300 s of the 2 hour measurement, the standard deviation is only  $9.0 \cdot 10^{-6}$  W which gives an error of 0.062 percent compared to the average of 0.0146 W. For the 45 minutes measurement, a small(er) drop in temperature can be observed again. An explanation could be that the room had to acclimatize again only now the temperature gradient between the hallway and the room in question was less. The different average power between the two separate measurements can be explained due to the overall temperature for the 45 minute measurement being lower than for the 2 hour measurement. The ambient temperature for the 45 minute measurement was 22 degrees Celsius while the temperature for the 2 hour measurement was 24 degrees Celsius. The standard deviation for the 45 minute measurement is  $1.4 \cdot 10^{-5}$  W which compared to the average of 0.0128 W is only a 0.11 percent error.

### 3.4 Sensitivity

In section 3.1, it is shown that the total measured power can be described as the system temperature  $T_{sys}$ . This temperature has an RMS uncertainty  $\sigma_T$  which is given by the radiometer equation, Eq. 3.11 where  $\Delta\nu$  is the bandwidth and  $t$  is the integration time.

$$\sigma_T = \frac{T_{sys}}{\sqrt{\Delta\nu t}}. \quad (3.11)$$

This RMS uncertainty can be seen as the sensitivity of the system, the lower limit of the source-temperature to be distinguished from the noise. As can be seen in Eq. 3.11, the higher the system temperature, the lower the sensitivity and the larger the integration time or bandwidth, the better the sensitivity.

For the single dish, we take the system temperature to be 300K. This is based on measurements with similar setups and so is assumed to be a realistic value. The integration time is 40ms and the bandwidth is approximately 1 GHz. Filling this into Eq. 3.11 we find that  $\sigma_T = 0.047$ K.

For a two element interferometer, Eq. 3.11 is modified into

$$\sigma_T = \frac{T_{sys}}{\sqrt{2\Delta\nu t}}. \quad (3.12)$$

For the interferometer, a filter is used causing the bandwidth to decrease to 40 MHz. Using the same system temperature and integration time we find that  $\sigma_T = 0.17$ K which is still quite all right for our measurements. Now we can translate this temperature to a flux density using

$$\sigma_s = \eta' \frac{2k}{A_{eff}} \sigma_T, \quad (3.13)$$

where  $\eta'$  is an efficiency factor of approximately 1 (Wilson, Rohlf, and Hüttemeister, 2013).

Plugging in our found values, we find that our sensitivity equals  $\sigma_s \approx 600$  Jy. According to (Sweijen, 2015), this would imply that the Sun and moon are easily visible with our setup at approximately 11 GHz. Other (radio-bright) astrophysical sources such as Cassiopeia A, Cygnus A and Taurus A are all too faint to be detected for  $\tau_0 = 0.01$ . If the filter is not used, a  $\sigma_s$  of 238 Jy can be achieved (neglecting efficiency's and atmospheric opacity) making it theoretically possible to detect Taurus A with a flux density of 509 Jy. The sensitivity could even be further increased by extending the integration time to seconds, making objects such as Cassiopeia A also visible.

### 3.5 Allan variance

Now using the stability measurements as shown before, the Allan variance and time can be calculated. Allan variance, also known as two sample variance is a measure of frequency (in)stability used in clocks, oscillators and amplifiers and is named after David W. Allan who published this technique in 1966. The Allan variance is an estimation of stability due to noise rather than systematic errors or environmental errors such as temperature effects. To determine the Allan variance, a data set is divided in bins based on an averaging time. Next, the average of each bin is calculated and compared with the consecutive averages of each bin. The difference between the bin and the consecutive bin is squared and all of the squares are summed up. At last, the sum is divided by the total number of bins returning the Allan variance as a function of averaging time. The mathematical definition is given by

$$\sigma_y^2(\tau) = \frac{1}{2} \left\langle (\bar{y}_{n+1} - \bar{y}_n)^2 \right\rangle \quad (3.14)$$

In this equation  $\langle \dots \rangle$  denotes the expectation value: the sum of the square of the differences between each bin, divided by the number of bins.  $\bar{y}_n$  is the n-th fractional frequency averaged over time  $\tau$ . The samples are taken without dead-time in between them, setting the time between 2 measurements  $T$  equal to the observation time  $\tau$ . Therefore there is no time after a measurement at which the system is unable to measure again.

Furthermore analog to standard deviation and variance, the Allan deviation is given by

$$\sigma_y(\tau) = \sqrt{\sigma_y^2(\tau)}. \quad (3.15)$$

A typical representation of the Allan Variance can be seen in figure 3.5. The noise contributions are also described. At first the Allan variance start decreasing as the noise domination is due to the power-sensor. At longer averaging times the variance decreases and finally increases again. The minimum of the variance is at the Allan time (where the Allan variance is the lowest) just before the random walk noise starts to dominate. The Allan time is the best integration time i.e. the integration time where least noise due to frequency instability is present.

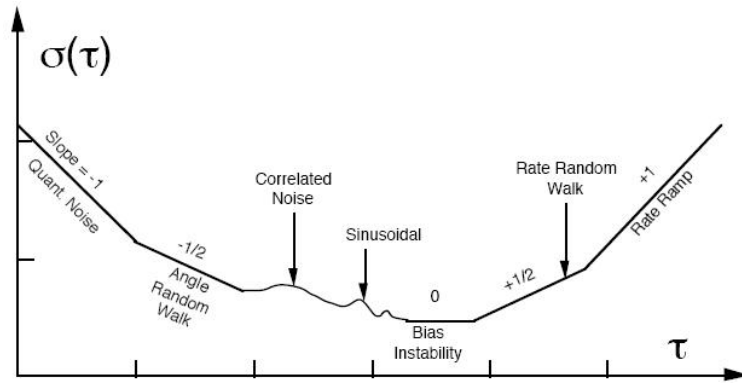


FIGURE 3.5: Noise contributions to the Allan deviation in a typical frequency standard. Image source: [Electronic Stackexchange](#)

For the stability measurements seen in figure 3.4, the Allan variance was calculated. Using the method described above and the python script given in Appendix B, Allan Variance plots were made which can be seen in figure 3.6 and 3.8.

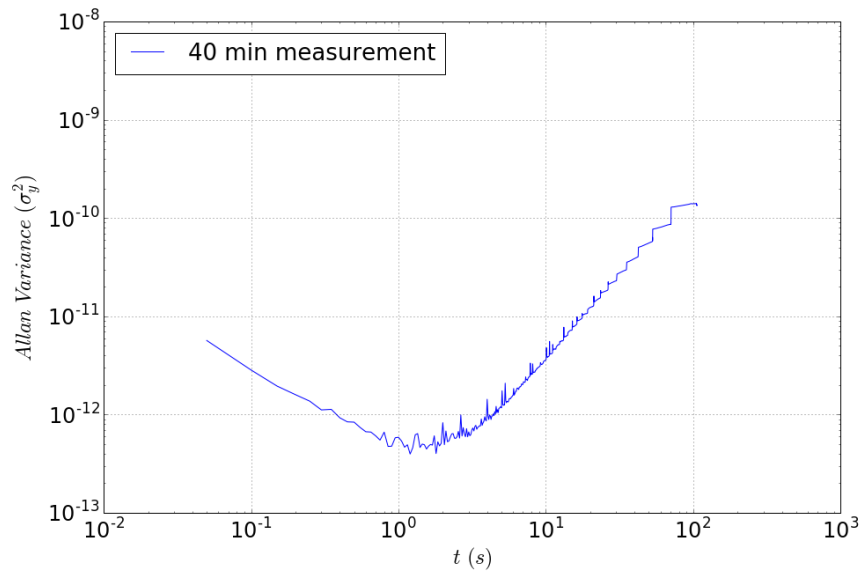


FIGURE 3.6: Allan Variance plot for a 40 minute stability measurement with an integration time  $\tau_0$  of 50 ms.

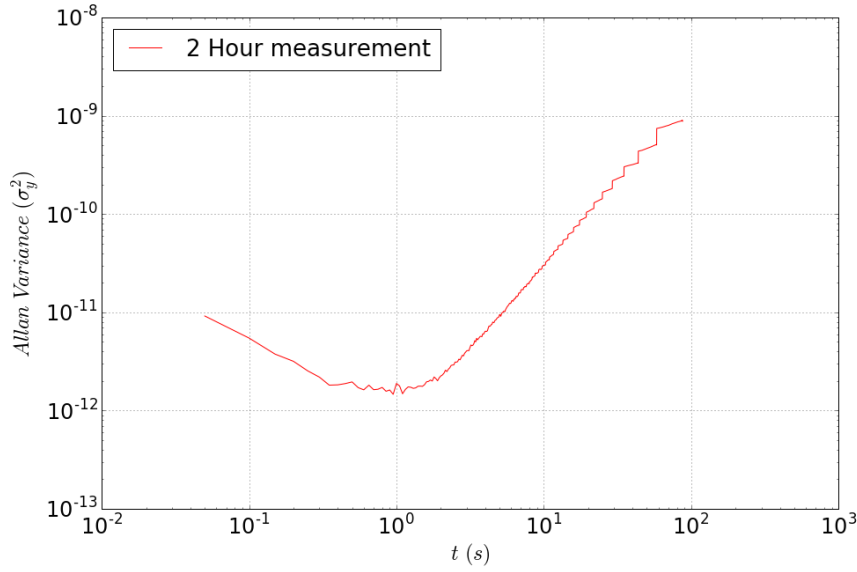


FIGURE 3.7: Allan Variance plot for a 120 minute stability measurement with an integration time  $\tau_0$  of 50 ms. Only the last 40 minutes were taken into account because this was the most stable part.

One can clearly see that for both measurements the profile is quite similar to that in figure 3.5. The Allan variance is first decreasing with a power law till a certain minimum (the Allan time) and then increases as another power law. The plots look almost identical to each other and show a clear minimum at approximately 1 second of integration time, in other words, the Allan time is 1 second. This means that an observation is most accurate (Allan variance of  $\sim 10^{-12}$ ) when the duration is close to 1 second. When doing a calibrated measurement such as a tip scan to determine  $\tau_0$  and/or  $T_{CMB}$ , the total measurement should not take much longer than 1 second before calibrating again to achieve the highest accuracy. Unfortunately this is not realistic, for our setup it takes at least a few minutes to finish the tip scan so we are far from our optimum. Nevertheless at an observing time of a few minutes, the Allan variance is  $\sim 10^{-9}$  which is still very low. If we compare our findings with those of Zandvliet (Zandvliet, 2015) and Formsma (Formsma, 2017), it seems that our setup has a higher stability. Zandvliet and Formsma both found an Allan time of  $\sim 10$  s for their system which is more convenient for tip scans. Nonetheless, their minimum Allan variances are  $\sim 10^{-9}$  and  $\sim 10^{-8}$  respectively which is quite high (in the order of 3/4 magnitudes higher) compared with our findings. To conclude, the time of observation used in measurements is not that relevant since the increased noise in regions far from the Allan time is still relatively small.

The radiometer equation, Eq. 3.11 can be rewritten into

$$\frac{\sigma_y^2}{T_{sys}^2} = (\Delta\nu t)^{-1}, \quad (3.16)$$

where  $\sigma_y^2$  is the Allan variance.

We can now fit this profile to our Allan plots to determine the effective bandwidth of our system. The radiometer equation can be fitted to the part where white noise is dominant, e.g. the first part of our Allan profiles. The Figure showing the Allan plots and their 'best' radiometer equation can be found in Fig. 3.8.

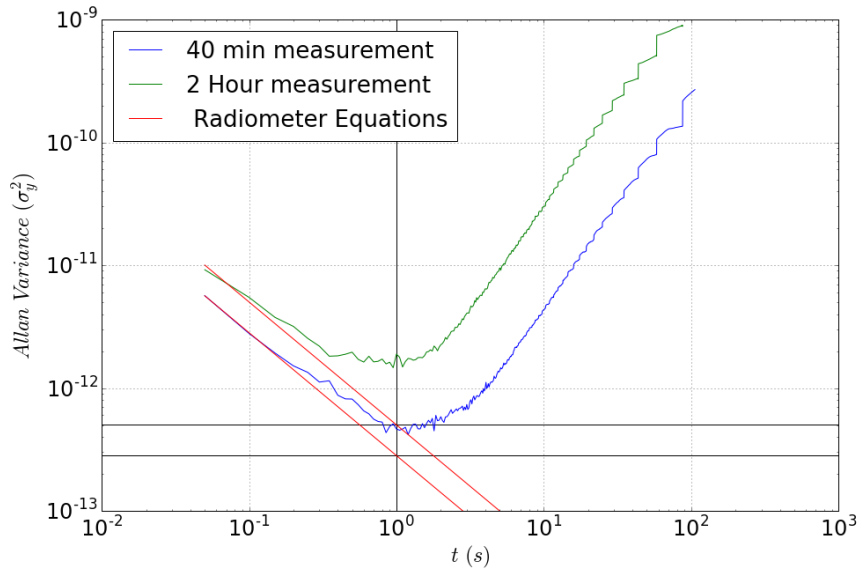


FIGURE 3.8: Allan Variance plots with their 'best' radiometer equation.

From section 3.3 we know that the average power ( $T_{sys}$ ) for the 2 hour measurement is equal to 0.0146 W and for the 40 min measurement 0.0128 W. The black lines corresponds to the Allan variance at a integration time  $t$  of 1 ( $10^0$ ) s of  $10^{-12.30} \text{ W}^2$  and  $10^{-12.55} \text{ W}^2$  for the 2 hour and 40 min measurement resp.

Knowing the integration time  $t$ , system temperature  $T_{sys}$  and allan variance  $\sigma_y^2$ , there can be solved for the bandwidth  $\Delta\nu$  using Eq. 3.16.

The effective bandwidth for the 2 hour measurement was found to be 425 MHz. For the 40 minute measurement, the effective bandwidth was found to be 581 MHz.

These findings imply that the effective bandwidth is approximately half of what the expected bandwidth should be.

## Chapter 4

# Radiation-and illumination pattern

### 4.1 Radiation pattern

Another valuable property of the single dish configuration is its radiation pattern. There are two methods to achieve the radiation pattern of a dish. One is to do a scan in the near field and by transforming it to the far field. The other is simply by determining the pattern by using a point source in the far field. The far field or FF is the region where the electromagnetic field of a transmitting antenna is a relatively uniform and isotropic wave pattern. On the other hand, the angular field distribution in the near field depends on the distance so that the field is anisotropic. The region where the far field starts is in the study of antenna design commonly given by the Fraunhofer distance as can be calculated according to

$$d_f = \frac{2D^2}{\lambda}, \quad (4.1)$$

where  $D$  is the diameter of dish and  $\lambda$  is the observing wavelength. For this equation to hold, the two conditions which have to be satisfied are  $d_f \gg D$  and  $d_f \gg \lambda$ . In our case we find that  $d_f$  is equal to 9.15 m.

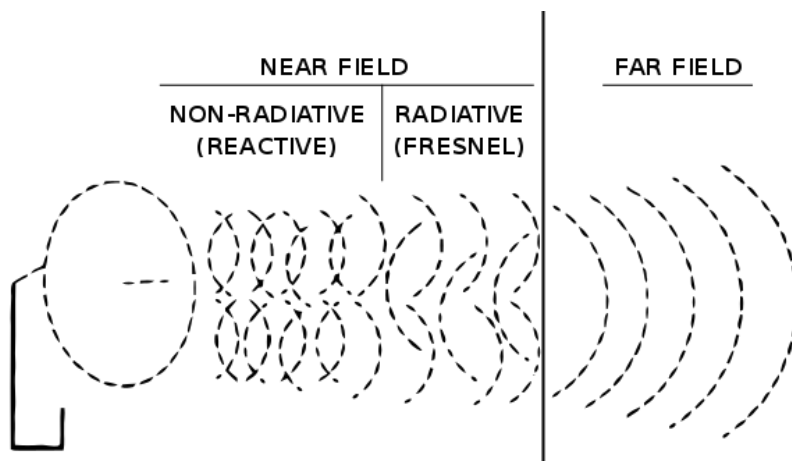


FIGURE 4.1: Figure showing the wave-propagation in the Near field and Far field. Image source: [wikipedia](https://en.wikipedia.org/wiki/Fraunhofer_distance)



#### 4.1.1 Far field scan

To practically determine the beam pattern one could use a point source emitting in the far field. The next step would be moving the receiver so that it sweeps past the source. Some important aspects are that the source must be much stronger than the background 'noise'. An obvious example is using digital video broadcasting satellites such as the ASTRA satellites from SES Astra. These satellites move in a geosynchronous orbit operating at a height of almost 36.000 km while the size is only a few meters. Due to these dimensions, the satellite can be approximated as being a point source. All DTV-satellites operate at approximately 11 GHz which is our frequency of interest. This is of course no coincidence because our frequency choice is based on the commercial LNB's made for receiving DTV signals. The power meter should give a Gaussian response to the sweep. From this Gaussian, the Full Width Half Maximum or FWHM can be determined which would represent the beam width of the main lobe.

On the 18th of May the first measurement to determine the beam width was done. The sky was scanned from an elevation of 20 degrees up to 60 degrees with steps of 3 degrees in between. The power displayed on the power meter was written down and afterwards a plot was made of the power response. Using a fitting script from the [SciPy](#) module, a Gaussian-profile was fitted and the standard deviation of the fit was returned. By making use of the fact that for a Gaussian the Full Width Half Maximum is given by  $FWHM = 2\sqrt{2\ln 2}\sigma$ , the Beam width was found to be 4.62 deg.

On the 30th of May the second measurement was done by making use of the Raspberry pi so that the output would have better accuracy. The turning nobs of the mount were twisted 90 degrees every 5 seconds so that the time (output) component could be converted to elevation angle (the time steps had to be multiplied by the total angle over the total time ratio). The output of the measurement with the Gaussian fit can be seen in [Figure 4.2](#) where the background is subtracted from the profile.

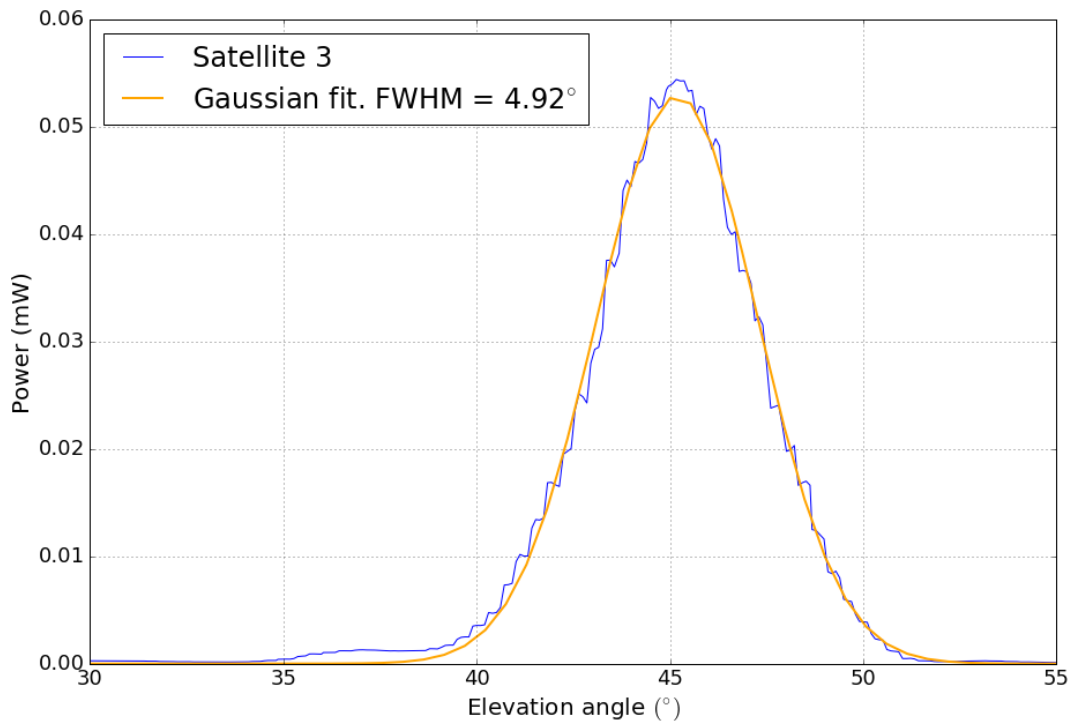


FIGURE 4.2: Power response of the signal coming from a point source in the far field with a Gaussian fit with FWHM= 4.92 deg.

One can clearly see that the Figure is not continuous but shows small (time) steps due to the twisting by hand per time step. A straight line between and elevation angle of 37 and 39 degrees can be seen which can be explained by the turning knob being stuck against the mount. Despite this, the fit looks fine and a beam width of 4.92 degrees was found.

On the 19th of June the last two FF measurements were done. Using the new tracking devices, the measurement could be done without human interference. Two satellites on different elevation angles were used and again a Gaussian profile was fitted through the data as can be seen in the next Figure.

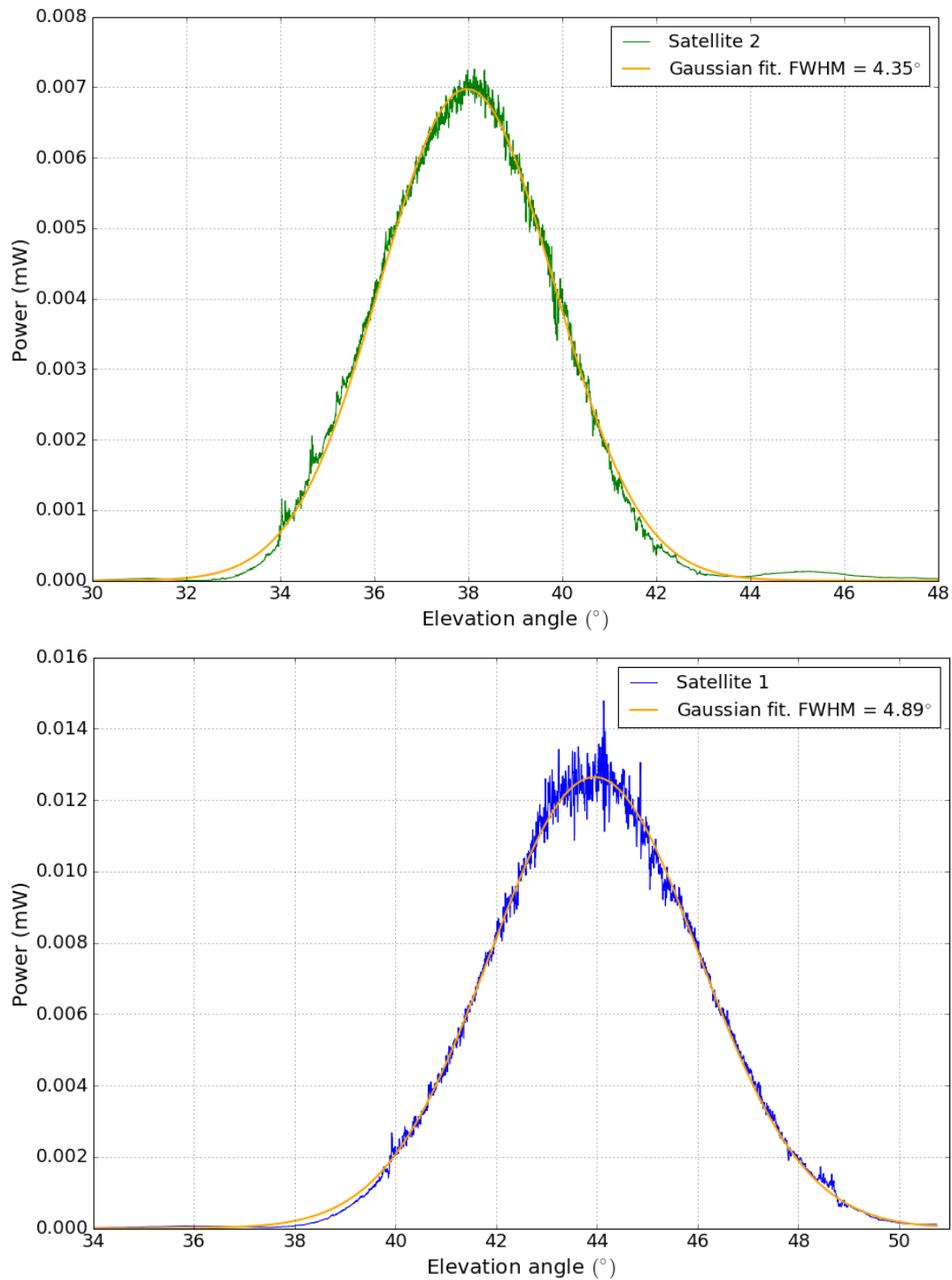


FIGURE 4.3: Power response of the signal coming from a point source in the far field with a Gaussian fit with FWHM = 4.35 and 4.89 degrees resp.

It can be seen that these plots contain a lot more data than the previous measurement due to the observation time being 50 times longer. Moreover, the total power for the second satellite is lower than for the first satellite. A reason for this can be that the centre of the beam does not go through the satellite or that the satellite radiates less. Furthermore the fit for satellite 1 seems to be more accurate than the for satellite 2 since it moves better through the Gaussian side structure. Additionally,

the overall power increases as a function of elevation angle so that it does not drop to zero again. This behaviour can clearly be seen in the top diagram of Figure 4.3 and can be explained by the atmospheric opacity. More atmosphere between the source and observer causes more attenuation and so, a lower received power. On the effect of the atmosphere on the measurements will be elaborated in section 5.1.

If the centre of the beam does not go through the satellite but rather radially extended from the centre, the Gaussian would decrease in size and the FWHM would also decrease. This would imply that the FWHM's found will only give a lower bound to the beam width. Since the geostationary orbit is almost completely filled with satellites emitting at our observing frequency, it is likely that there are multiple satellites in our field of view. As a result, the chance of having a satellite very close to the centre cross-cut of the beam is high which will dominate the Gaussian and so the largest FWHM's found will likely be close to the 'real' beam width. To conclude, the beam width is estimated to be approximately  $4.90^\circ$ . This beam width would correspond to a  $K$ -factor of 64.4.

At last, especially for satellite 1, side lobe structures are clearly visible. In Fig. 4.4 the measurement of satellite 1 can be found with horizontal and vertical lines indicating the location of main lobe and side lobe peaks

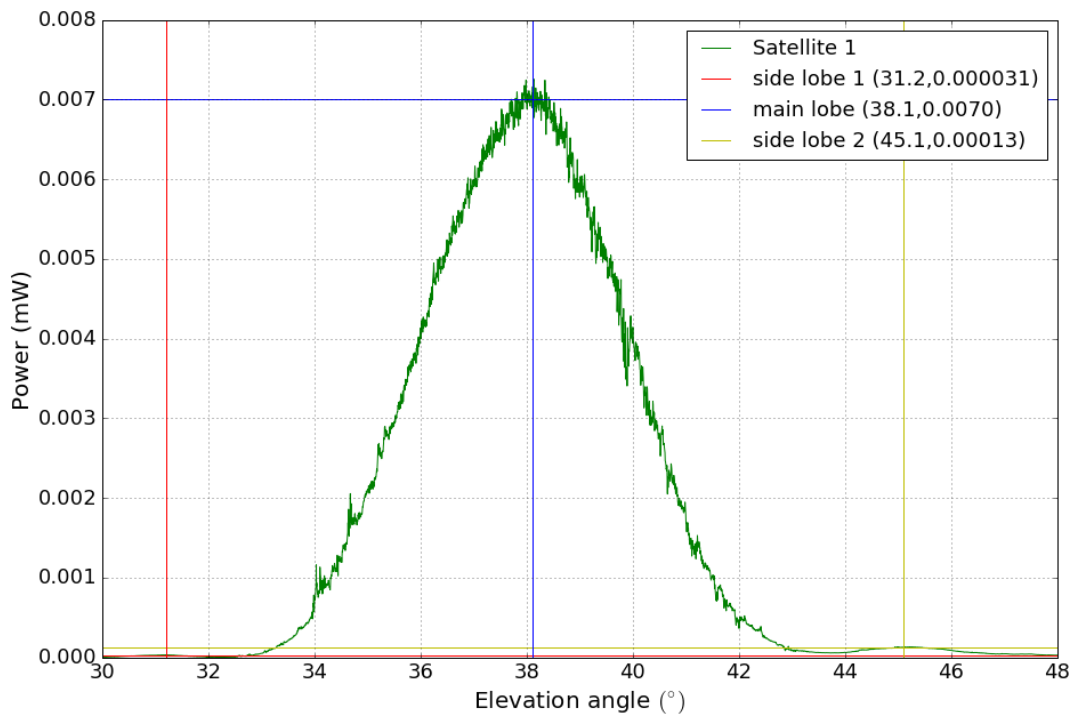


FIGURE 4.4: Power response of a satellite with horizontal and vertical lines indicating the peaks of the main and side lobes.

In this diagram the side lobe structures are not that visible but the coordinates of the peaks can be found in the legend. The Figure was shifted so that the elevation angle can be converted to offset angle from the main axis. By defining the top to be 0 dB and calculating the relative differences w.r.t. the top of the main peak in dB scale, Figure 4.5 was obtained.

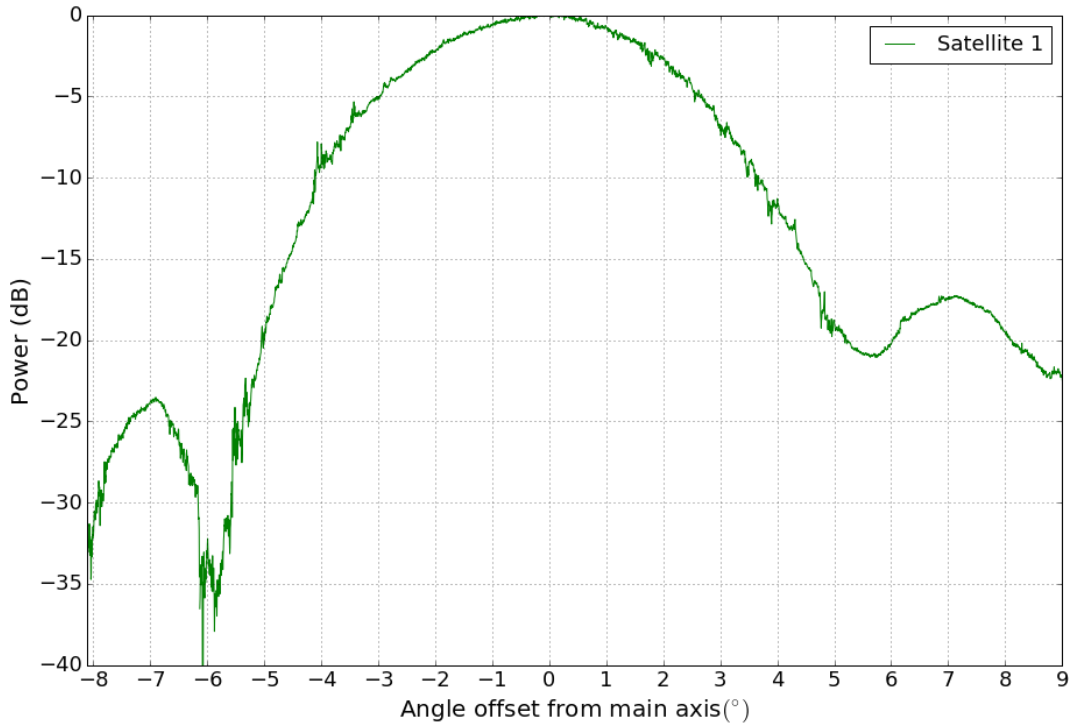


FIGURE 4.5: Diagram showing the beam response of the system in dB as a function of offset angle.

Because of the atmospheric opacity, the power at the negative offset angle is shifted downward with a certain degree. When subtracting the opacity, the left side lobe still gives a lower power response than the right side lobe which could also be due to asymmetry in the dish. We can conclude that the side lobes of the dish are at approximately 7 degrees from the main axis and have a relative response of approximately -17 dB (assuming the right side lobe is more accurate). According to literature, the beam pattern of our dish (if it was a perfect disk) should give a Bessel function of first order  $J_1$ . This would imply that the first null should be at an offset angle of  $\approx 5.3$  degrees and the peak of the first side-lobe at  $\approx 7.1$  degree which is in line with what can be seen in Fig. 4.5. Furthermore the peak of the first side lobe should be at -17.57 dB which is again, very close to our (-17.3dB) result. This found values suggest that our beam pattern seems to follow the Bessel profile very well. The side-lobe level of 17.3 dB suggests that the surroundings of the telescope have a major impact on the measurement. The side-lobes add an additional factor of  $2 \cdot 10^{\frac{-17.3}{10}} \approx 4$  percent to the total system temperature. When measuring an astrophysical source while the ambient temperature (of the surroundings) is 300K, this would mean that the side-lobes add another 12K to the total system temperature. This is a very dramatic results because this would imply that the CMB with a temperature of 3K could never be resolved unless the side-lobes are very well calibrated.

### 4.1.2 Near field scan

#### Setup

Another method used to obtain the radiation pattern is by doing a scan in the near field and transforming it to the far field. This was done using a Vector Network Analyzer or VNA. At first, a microwave generator outputs a signal which is transmitted by an antenna via a piece of wave guide. The signal is received by the LNB (via the dish) which is subsequently directed to the input of the VNA. The VNA is able to give information about the amplitude- and phase-response. Using a computer, an XYZ-table was operated so that the source can be swept in front of the dish to create an YZ-plane orthogonal to the beam (moving in the X-direction) of the dish. The phase and amplitude output is correlated with the varying location of the wave guide using a computer.

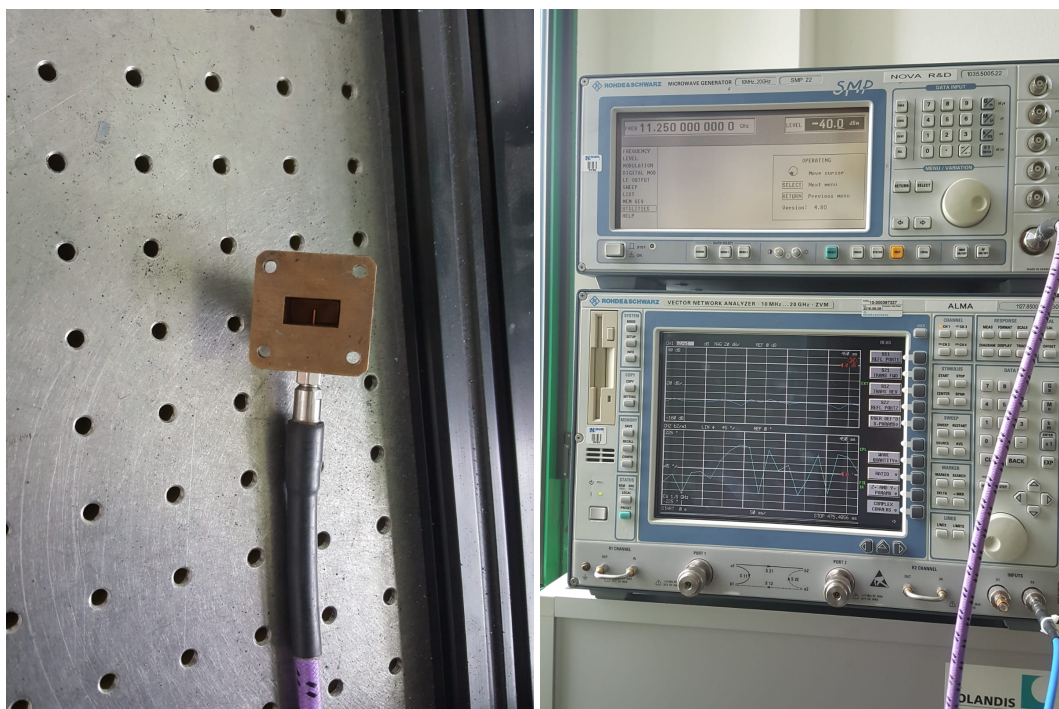


FIGURE 4.6: Picture showing the piece of wave guide on the left with the antenna clearly visible. The wave guide is connected to the microwave generator on top of the VNA on the right.

In our case the microwave generator was set to give an output of 11.25 GHz with a power of -40 dBm (Fig. 4.6.) The transmitted signal was directed onto the dish and reflected into the LNB. It was important to put the dish on the desired elevation angle of  $29^\circ$  to create a flat wave front. The flat wave front would give the right amplitude feedback which could be checked using the phase response. Furthermore the setup was surrounded by absorbing material to decrease standing waves. To mount the wave guide to the XYZ-table a piece of aluminum was processed so that it would connect the wave guide to the table using some screws. A rectangular piece of copper was constructed and soldered to act as an extension of the wave guide. This was done so that the radiation would go straight ahead and not interfere with the sides of the wave guide. Using the copper extension, the absorbing material could perfectly fit around the source. A picture of the final setup can be found in Figure 4.7 and 4.8. A diagram showing all the components and connections can be



found in Figure 4.9. The blue connection represents a phase locked loop, connecting the microwave generator, VNA and the signal generator so that the input phase can be compared to the output phase.

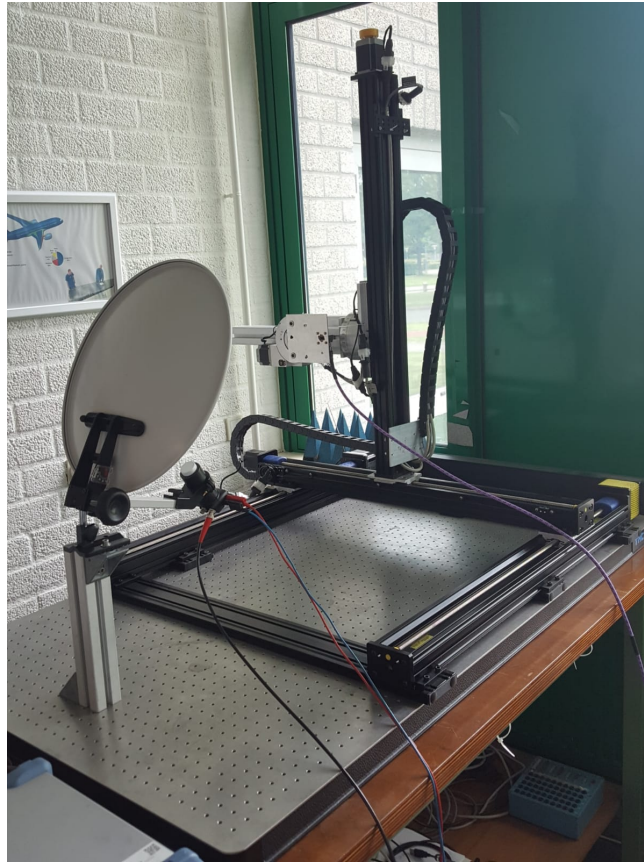


FIGURE 4.7: The setup used to do the near field scan showing the wave guide mounted to the XYZ-table.



FIGURE 4.8: The setup used to do the near field scan showing the copper extension and blue RF absorbing material.

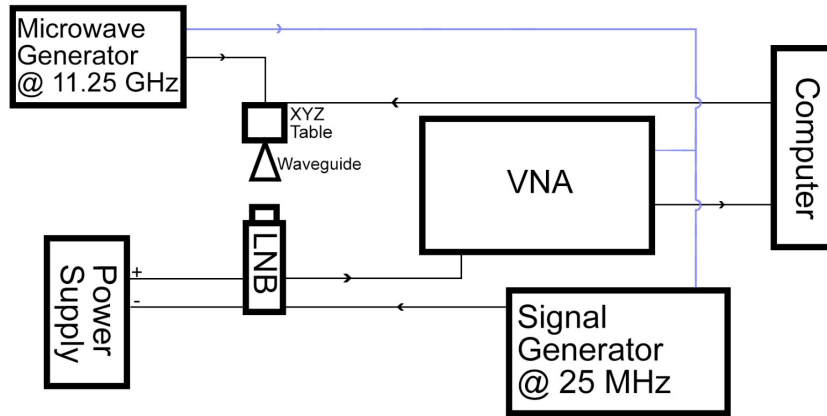


FIGURE 4.9: Diagram showing the setup for the near field scan. Image source: (Farret Jentink, 2018)

After each scan, another measurement was done using the same YZ-scanning plane but now with a shift in the X-direction of  $\frac{\lambda}{4}$ . The two data sets were combined by subtracting the shifted data, set multiplied by the imaginary unit and dividing the total by two. Using this method, standing waves could be eliminated. Using a Fourier transform, the combined near field data set was transformed to the far field. Using the python code (Appendix D) obtained from Lap (Lap, 2015), the data reduction was done to obtain the final beam widths.

From the 21th of May to the 8th of June, a total of 10 measurements were done resulting in 5 combined data sets. One scan using a y- and z-span of -17 to +17 cm with in both direction 65 steps resulting in 4225 data points. Three measurements were done using a span of -20 to + 20 cm with 81 steps on both axis resulting in 6561 data points. One measurement was done using the largest possible span of -25 to + 25 cm with 101 steps, resulting in 10201 data points. The highest accuracy can be achieved by maximizing the span of the observed YZ-plane (the span determines the step size in the Fourier transformed far field due to the Nyquist–Shannon sampling theorem). Nevertheless it was found that this gave hardly any better results. The data set of -20 to +20 cm gave the best results and will be used for further analysis in the next section.



## Results

The phase- and amplitude response can be found in Fig.4.10 and 4.11 respectively.

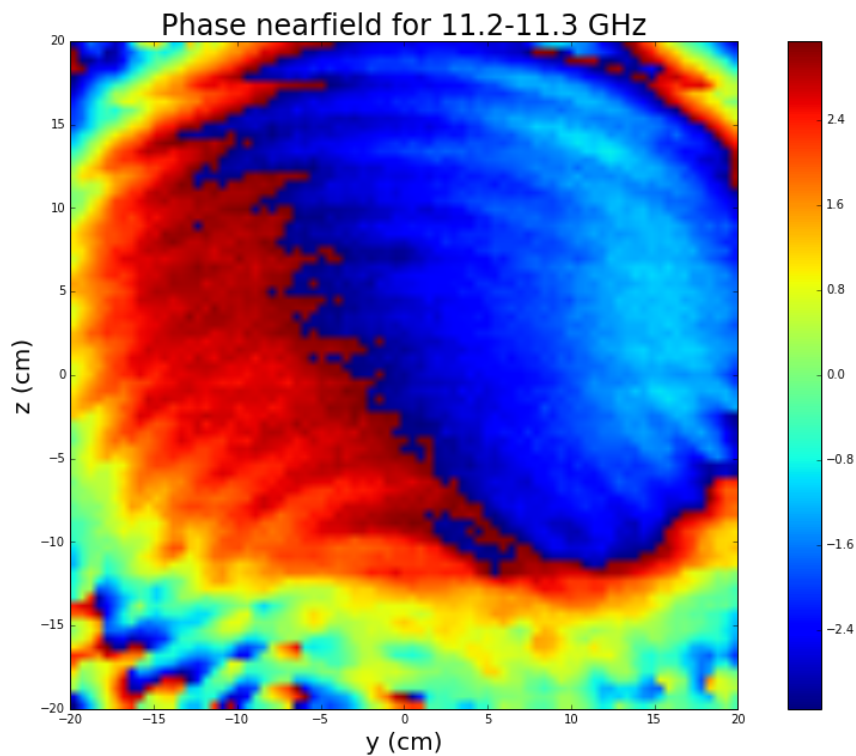


FIGURE 4.10: Figure showing the Phase response for the data set of -20 to +20 cm for both the y- and z-axis.

The phase looks almost flat, a slight tilt can be seen corresponding to a tilt of half a degree over the total aperture. Some standing waves are prominently visible as waves coming from the  $y=0$  cm and  $z=-20$  cm direction moving radially outward.

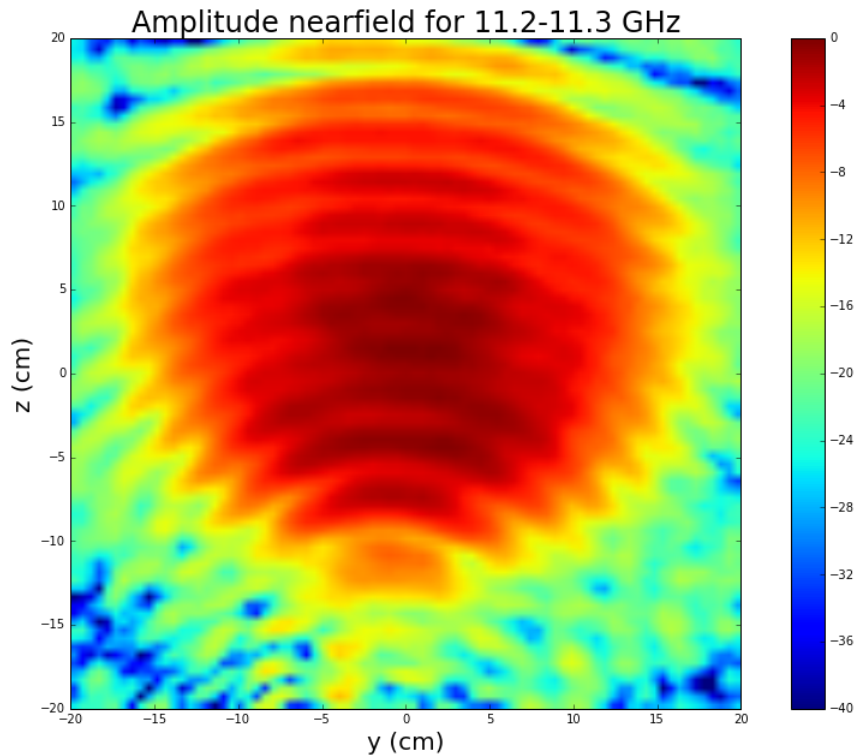


FIGURE 4.11: Figure showing the Amplitude response for the data set of -20 to +20 cm for both the y- and z-axis.

For the amplitude one can clearly see the nearly circular shape of the dish and amplitude falling off radially as expected. Again, the same standing waves can be seen as in the phase-diagram. The maximum cross cut of the amplitude can be found in Fig. 4.12.

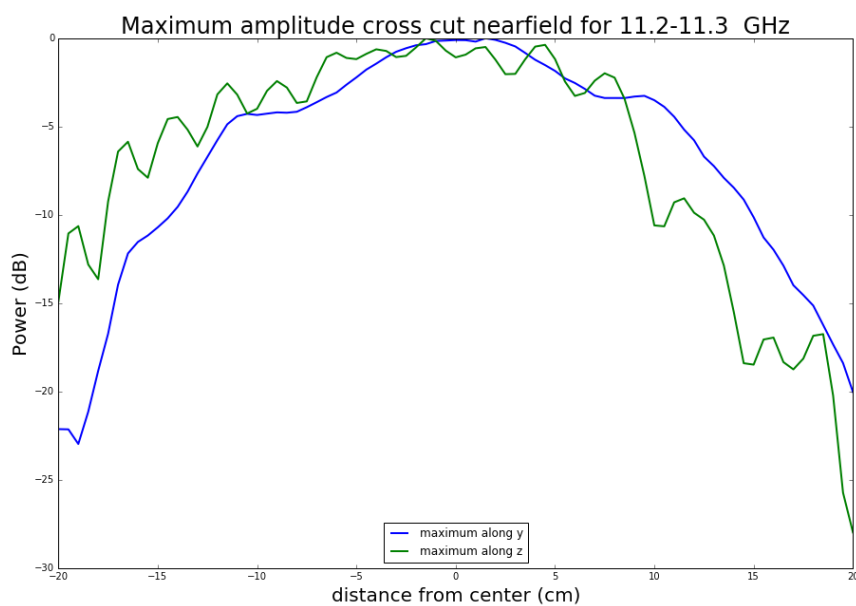


FIGURE 4.12: Maximum cross cut of the near field amplitude for both the y- and z-axis

From this Figure it is clearly visible that the y-direction is far more symmetrical

than the z-direction. One can see that there is one main lobe with 2 clear side lobes for the y-direction. For the z-direction there is quite a lot of asymmetrical side lobe structure which is probably due to interference on the asymmetrical axis of the dish. At the end of the positive z-axis, there are sudden drops due to the LNB obstructing the beam causing a drop in power. The Fourier transformed (far field) amplitude response can be found in Fig. 4.13

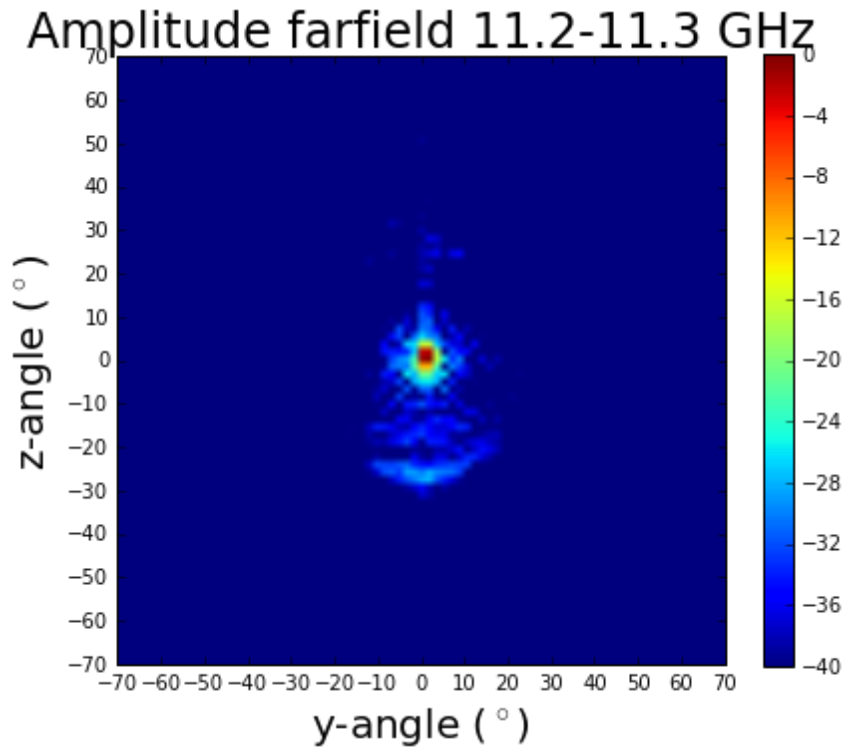


FIGURE 4.13: Far field amplitude response for an angle of  $-70^\circ$  to  $+70^\circ$  for both the y- and z-axis.

The image clearly shows the main beam being in the centre, some side-lobe structure can be seen dominantly in the z-direction. The large blob at approximately  $-25^\circ$  can be explained by the LNB being in the beam. The maximum cross cut of the far field amplitude can be seen in Fig. 4.14

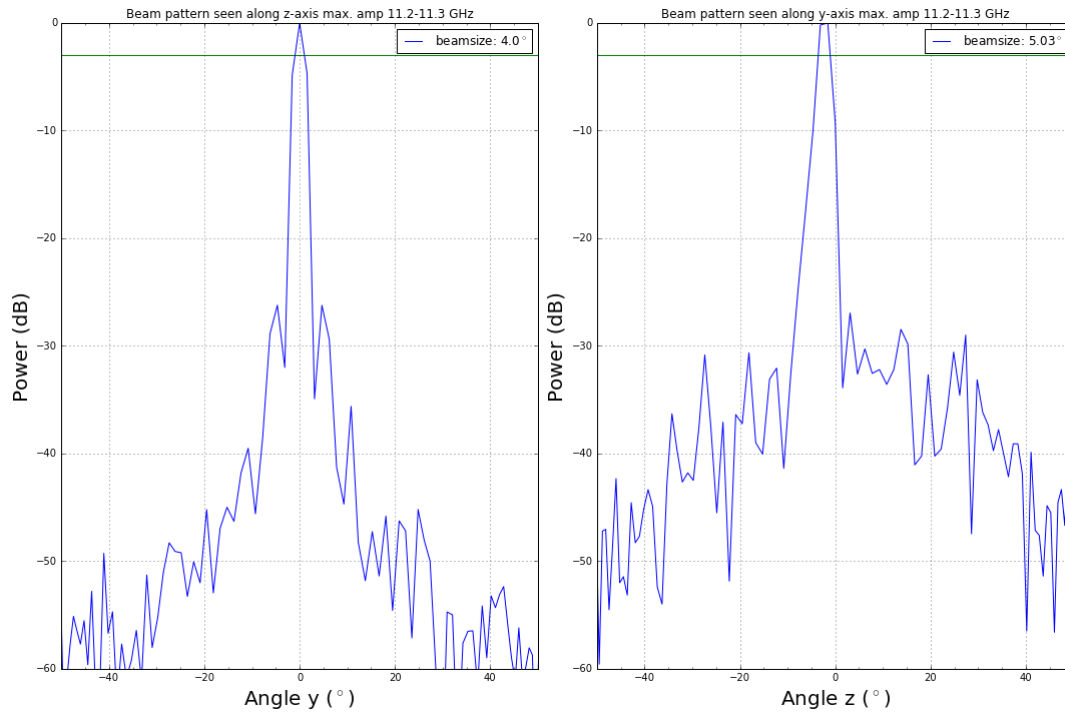


FIGURE 4.14: Figure showing the maximum amplitude response for both the y- and z-axis in degrees.

This Figure shows the final radiation pattern for both y- and z-direction. The green lines corresponds to the -3dB drop or the beam width. The beam width in the y-direction was found to be  $4.0^\circ$  and  $5.0^\circ$  for the z-direction. The first side-lobes are clearly visible at an offset angle of approximately 5 degrees from the main axis for the y-direction. For the z-direction it is hard to distinguish side-lobes, together with the skewed main lobe it can be concluded that the y-axis is far more accurate. For 2 other measurements, the beam width of the y-axis was found to be  $4.0^\circ$  for both measurements, implying a precise result. For the z-axis, fluctuating beam widths of  $6.89^\circ$  and  $8.09^\circ$  were found, implying low precision. For the (maximum) far field plots the accuracy is evidently low. Looking at the number of data points, it is obvious that higher accuracy could be reached by maximizing the span. Nevertheless the total span could not be larger than -25 to +25 cm for both axis. Due to this reason it can be concluded that the beam width found using the far field scan gave (as expected) the most accurate result.

## 4.2 Illumination pattern

The illumination pattern describes how the dish is illuminated by the LNB and so influences the final radiation pattern. The most accurate results are achieved when the dish is evenly illuminated by the LNB so that the final radiation pattern is only dependent on the dish. In practice this can never be achieved. The maximum efficiency (minimum spillover compared to maximum gain) is obtained when the edge or rim of a circular aperture is illuminated with -11dB. In practice, an edge taper of -10 dB is said to give the optimal result (NCRA-TIFR, 2002). From previous measurements we found that there is a lot of spillover so it was interesting to investigate our illumination pattern.

Using the same measurement setup as for the total radiation pattern, the illumination pattern was obtained. The observing frequency was again 11.25 GHz and a scanning field of 28 cm times 28 cm with 50 measurements on both spatial(y,z) directions was chosen with a separation between the source (rectangular tube) and LNB of 15 cm as visible in Fig. 4.15.



FIGURE 4.15: Start position of the scanner, a field of -14cm to +14 cm for both y- and z-direction were chosen.

The phase and amplitude responses can be found in Fig 4.16 and 4.17 respectively.

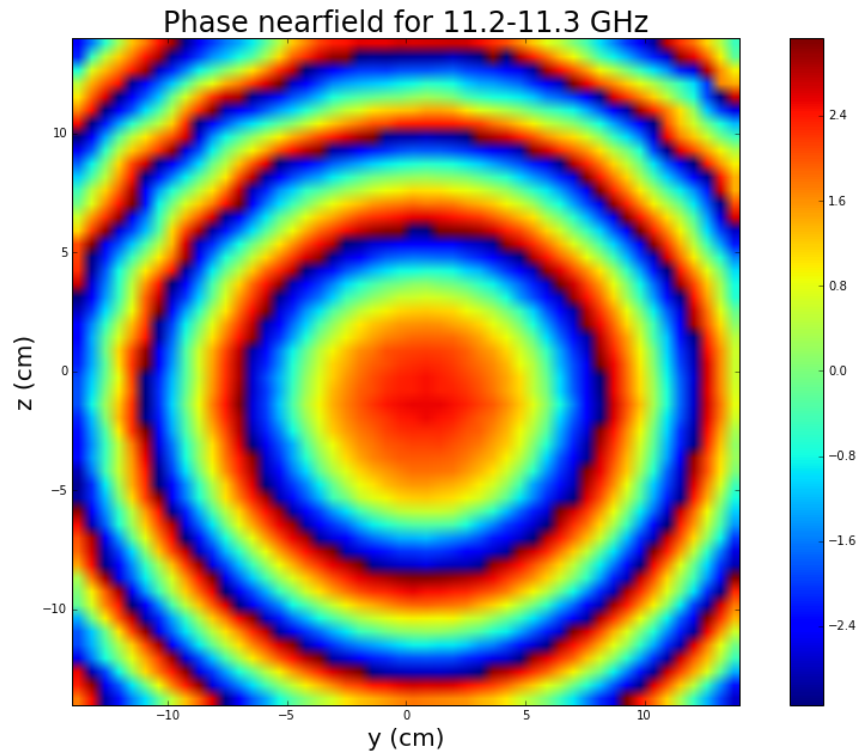


FIGURE 4.16: Near-field phase response for the LNB at 11.25 GHz.

From this diagram we can clearly see that the LNB was placed in the right way without an angular offset. The phase should give a circular distributed response (for a circular aperture) just as visible in Fig. 4.16. There is a small spatial offset towards the +y and -z direction which is irrelevant for our measurement.

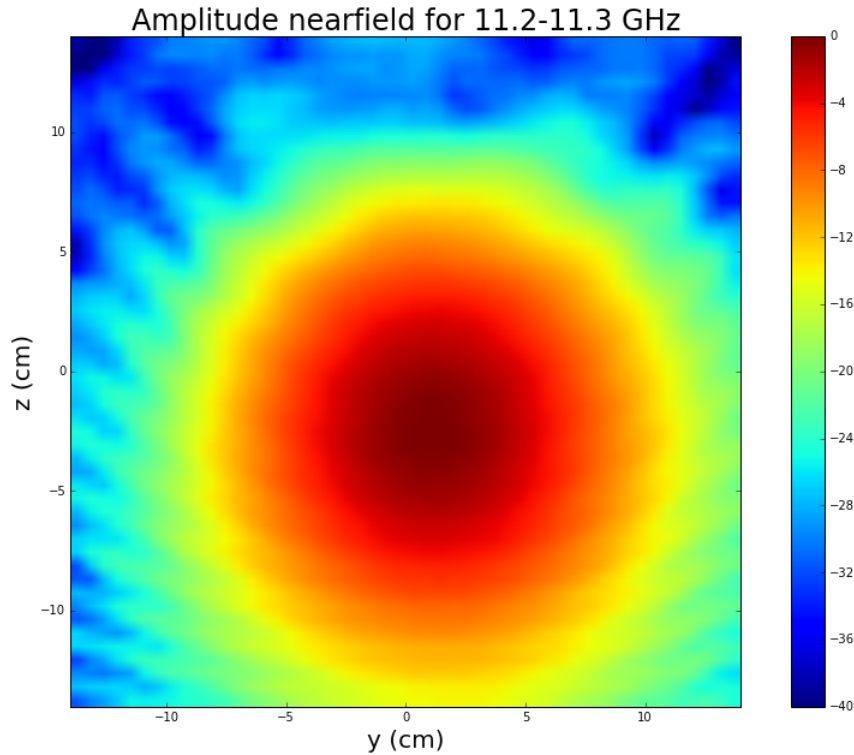


FIGURE 4.17: Near-field amplitude response for the LNB at 11.25 GHz.

From the amplitude response it is visible that there is indeed a small offset towards the +y and -z direction. There are again some standing waves visible in the diagram. The maximum crosscuts in y- and z-direction of the far field amplitude plot can be seen in Fig. 4.18.

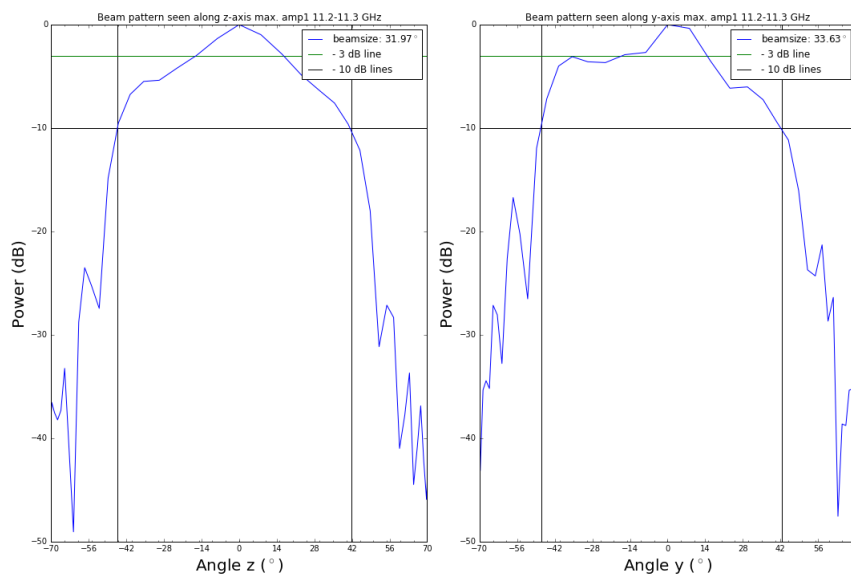


FIGURE 4.18: Maximum cross cut of the amplitude in y- and z-direction representing the beam pattern of the LNB.

The Figure shows a relatively evenly illuminated pattern. The resolution of the plot is quite good comparing it with the of the dish due to a relatively large scanning



span. The beam width ( $-3\text{dB}$ ) is found to be  $33^\circ$  on average and the  $-10\text{dB}$  angle is approximately  $90^\circ$ . Looking at the beam patterns, it can be concluded that this result is not very precise due to a lack of measurement points. In Figure 4.19 the illumination onto the dish can be seen where the LNB is pushed inward as far as possible.

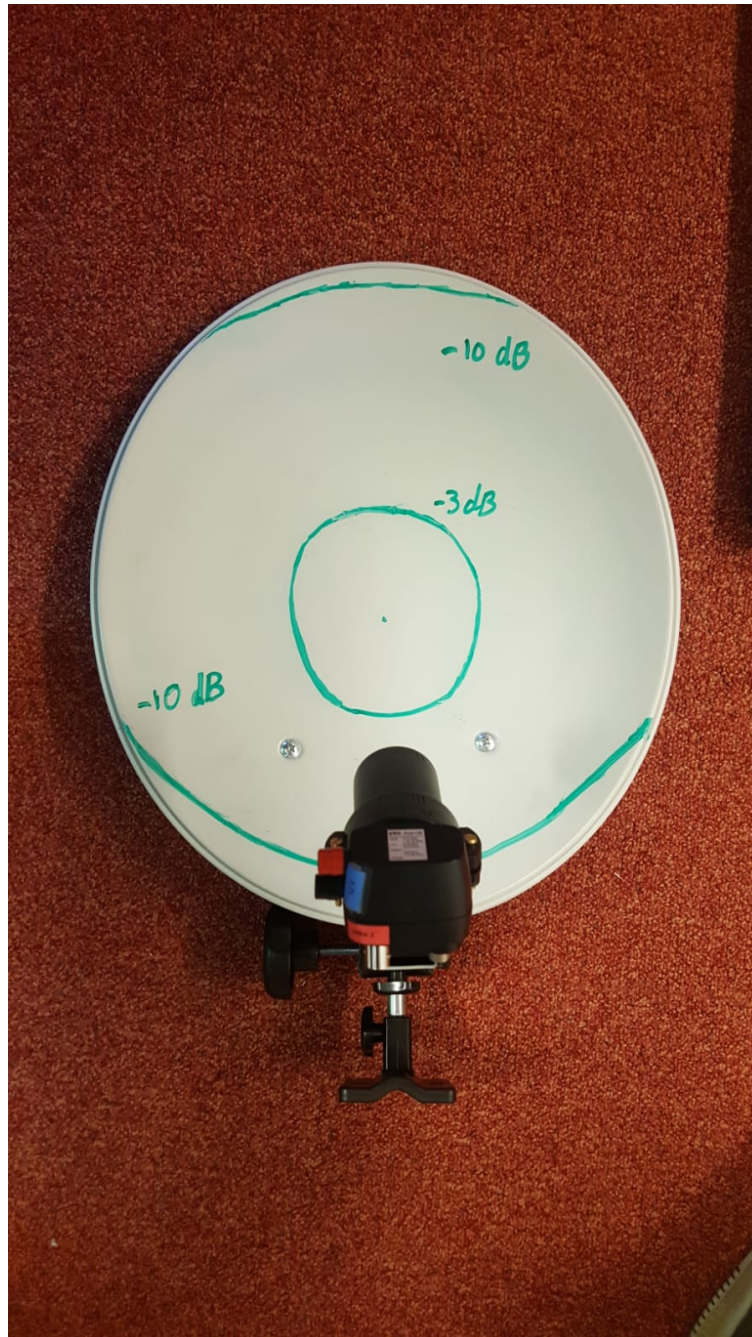


FIGURE 4.19: Front view image of the dish showing the projected angles of the  $-3\text{dB}$  and  $-10\text{dB}$  spread.

In this Figure it is shown that the edge illumination of  $-10\text{dB}$  is reached quite all right. From this we can also conclude that the cold load in section 3.2 did not fill the entire beam because the LNB was subtracted approximately 4 cm, causing a lot of spillover.



### 4.3 Aperture efficiency

Using the phase output (Figure 4.20) discussed before, the RMS of the surface deviations of the dish was determined. At first, the phase difference was converted to an optical path length difference (OPD) following

$$\Lambda_{opd} = \frac{\lambda \Delta\phi}{2\pi}, \quad (4.2)$$

where  $\Lambda_{opd}$  is the optical path length difference and  $\Delta\phi$  is the phase difference.

The phase plot has a slight systematic tilt so if the deviations from the mean would have been calculated right away, they would have been unrealistic. Furthermore, the beam is not completely covered by the scan and some of the surroundings are within the scan-area.

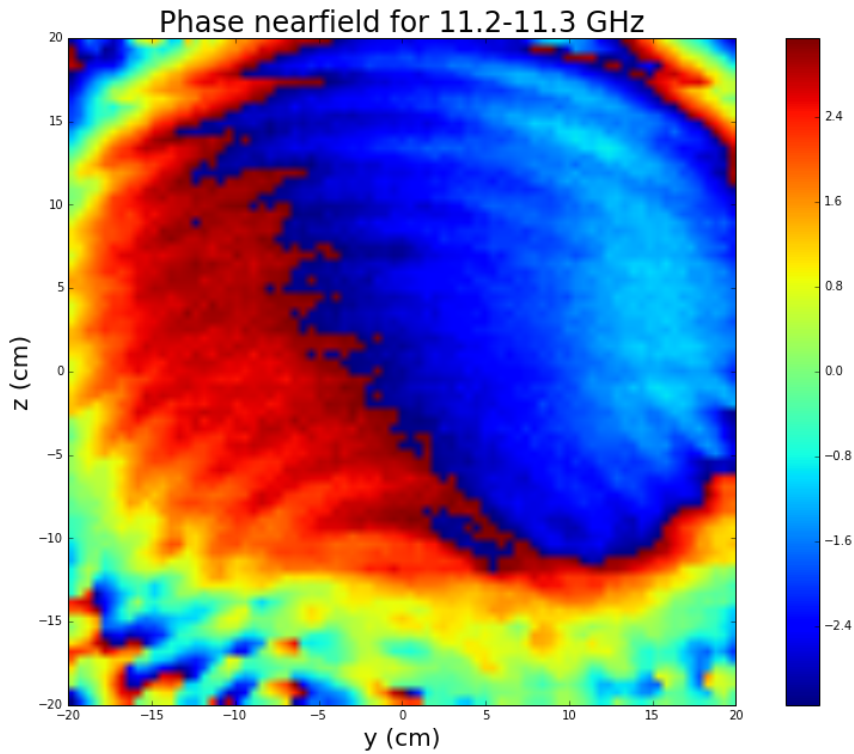


FIGURE 4.20: Phase diagram showing the differences in phase or arrival time for various locations on the dish.

The solution for this that first a few small parts of 3 by 3 cm (as close as possible to the centre) of the total covered area were taken apart. For these separate parts, the mean OPD was calculated. Following that up, the differences in OPD w.r.t. the mean OPD were calculated and squared. Next, the squares were summed and the total was divided by the number of squares. At last the square of the total was calculated which gave the RMS deviations as

$$\Lambda_{opd_{RMS}} = \sqrt{\frac{1}{n}(\Lambda_{opd_1}^2 + \Lambda_{opd_2}^2 + \dots + \Lambda_{opd_n}^2)}. \quad (4.3)$$

The RMS was found to be  $0.0447\lambda$ . Using Ruze's equation, an efficiency of 73 percent was found. In reality the efficiency is probably higher because of the overall tilt in the plot. The scanner measures the OPD every 0.5 mm meaning that the scan-area per part is only 6 times 6 measurements. If the overall tilt is approximately  $0.5^\circ$  this would already imply an OPD of 0.03 mm between the first and last measurement. Since the expected RMS per part is of the same order of this OPD, the calculated efficiency can only be used as an lower bound estimate.

According to section 3.2, the  $T_{rcv,LNB} = 113\text{K}$  while  $T_{rcv,dish} = 208\text{K}$ . From these values, the spillover of the LNB can be calculated. By making use of the fact that the cold load is 77.15 K while the surroundings are 295.25 K, one can calculate the spillover efficiency. Knowing that the temperature of the dish should equal  $\eta_{spill}$  times the temperature of the LNB plus  $(1 - \eta_{spill})$  times the surrounding temperature we find

$$\eta_{spill} = \frac{T_{sur} - T_{rcv,dish}}{T_{sur} - T_{rcv,LNB}}. \quad (4.4)$$

Using this equation,  $\eta_{spill}$  was found to be 0.48 so that the efficiency is only 48 percent. This result is very radical concerning that more than half of the beam is filled by the surroundings. For all future measurements, the LNB is placed as far as possible towards the dish to minimize the spillover (and so lower the gain).

## Chapter 5

# Elevation scan

### 5.1 Determination of $\tau_0$ and $T_{rcv}$

When radiation passes through the atmosphere, part of it is attenuated. How much of the radiation is attenuated is measured by the opacity  $\tau$ . The opacity is dependent on the path-length through the atmosphere and the optical depth of the atmosphere. The atmosphere can be approximated as being plane parallel with the earth's surface so that we can calculate the opacity by

$$\tau(z) = \frac{\tau_0}{\cos(z)}, \quad (5.1)$$

where  $\tau_0$  is the optical depth at zenith (assumed to be constant) and  $z$  is the zenith angle (measured from zenith to the horizon) as shown in Figure 5.1.

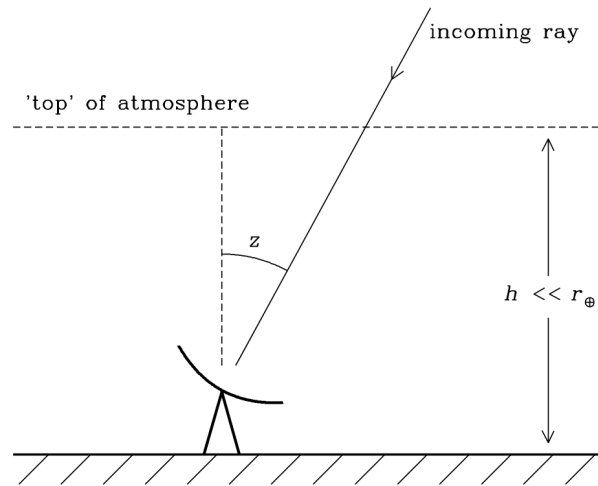


FIGURE 5.1: A simple model of the atmosphere to determine the opacity  $\tau$  as a function of zenith angle  $z$ . Image source: [NRAO](#)

Besides, the receiver temperature of the LNB + dish will again be determined but now with the LNB pushed as far as possible towards the LNB to minimize spillover. The output of the second measurement can be found in Figure 5.3 where the zenith angle is the angle between zenith and the measured angle. At zenith, the zenith angle is zero degrees and at the horizon the zenith angle is 90 degrees. The expected exponential profile is clearly visible between 0 and 80 degrees. Outside of this range, the response is unrealistic and is neglected for further research.



FIGURE 5.2: Left: The LNB is pushed inward to minimize spillover. Right: The sky in the (North) direction in which the observation was done, clouds are predominantly.

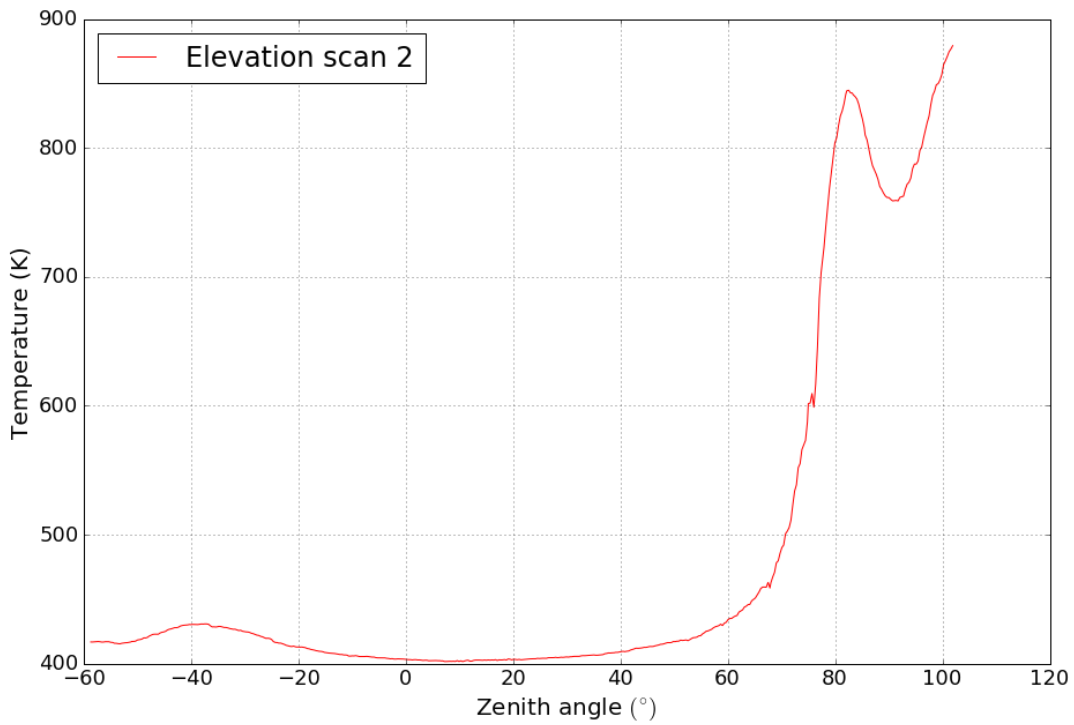


FIGURE 5.3: Figure showing the power (brightness temperature) response as function of zenith angle.

Using the brightness distribution, Nyquist theorem given by Eq. 3.1 and Rayleigh-Jeans law (Eq. 1.5) the following profile was found for the measurement of a distant source through a slab of atmosphere:

$$T_b(s) = T_b(0)e^{-\tau(s)} + T(s)(1 - e^{-\tau(s)}) \quad (5.2)$$

(Mulder, 2015).

In our case we can substitute  $T_{CMB}$  for  $T_b(0)$ ,  $T_{sky}$  for  $T(s)$  and  $T_{ant}(z)$  for  $T_b(s)$  where  $z$  is the zenith angle. A fit of the exponential profile was made for our elevations scans. Using the gain found in the previous section and by making the assumption that the temperature of the CMB is 2.7K, there could be solved for  $\tau_0$  and  $T_{rcv}$ .

Only the part from approximately 0 to 25 degrees was used for the fit because this gave the best fit to the data, see Figure 5.4.

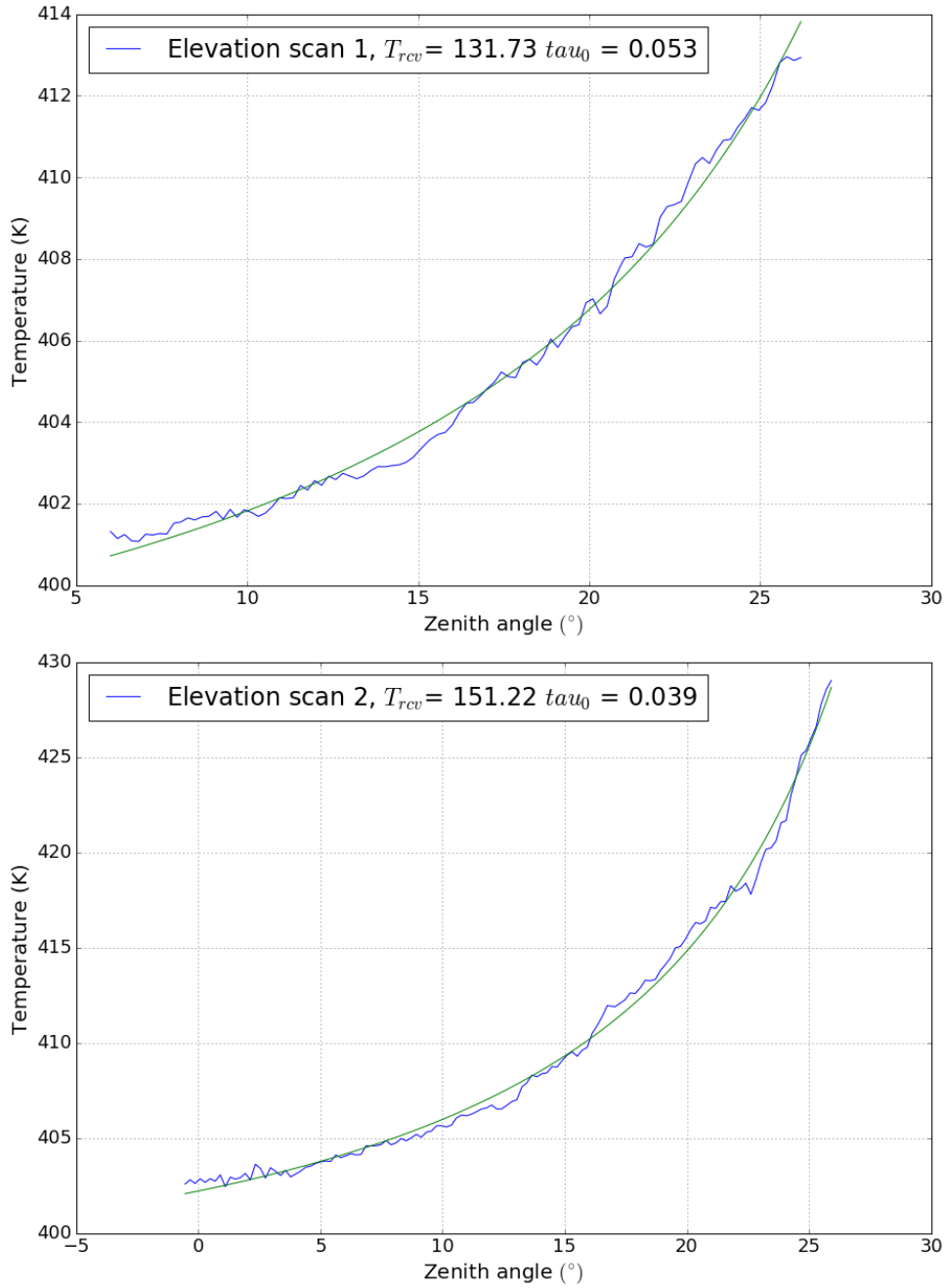


FIGURE 5.4: Figure showing the power responses as function of zenith angle with exponential fits.

The fit returned that the opacity at zenith  $\tau_0$  is 0.053 and 0.039 for scan 1 and 2 respectively. The opacity at zenith seems to be somewhat large if we compare it with the values found by (Formsma, 2017) and (Mulder, 2015), 0.019 and approximately 0.03 resp. This difference could be due to the cloud layer above our observing location when the measurement was done. To determine the receiver temperatures, the CMB and sky temperature were subtracted from the system temperature. For the receiver temperature  $T_{rcv}$  we found 132 K and 151 K. These values differ somewhat from each other but are in line with what was expected. The found temperature is higher than for the LNB alone but lower than for the LNB + dish as measured before. Since the LNB was pushed as far as possible inside, the influence from the ground (spillover) was minimized. This could have caused a drop (from 208 K to 132/151 K) in receiver temperature for the LNB + dish.

## Chapter 6

# Conclusion and further research

### 6.1 Conclusion

The goal of this bachelor project was to construct the frontend of the Kapteyn Interferometer, i.e. adapting the mounts and dishes to ensure that the interferometer works. The equatorial mounts and offset parabola dishes are combined and together with the back-end and cabling, the interferometer was used to observe the sun.

Furthermore the single dish configuration was investigated.

The radiation pattern of a single dish was mapped, clearly showing side lobe structures with the expected power-levels implying that the dish is as good as useless to do calibrated measurements of radio quiet sources. The beam width was found to be approximately  $4.9^\circ$  and the side lobes are at a power level of -17.3 dB.

The Allan time was found to be approximately 1 second which is in line with results found for similar setups (Formsma, 2017). The effective bandwidth was found to be approximately 500 MHz which is half of the theoretical value (1 GHz).

The sensitivity of the single dish and interferometric setup were determined, implying that other astrophysical sources next to the sun and moon are unable to be observed unless the integration time is increased to the order of seconds.

The spillover efficiency was determined to be 48 % when the LNB was placed on the 'standard' intended location. For further measurements the receiver was placed as close as possible (in the clamp) to the dish, reducing the spillover and gain.

An aperture efficiency of 73% was estimated which is an unrealistic result and was not taken into account. The illumination pattern was researched which revealed a lot of spillover and the optimal LNB placing was determined.

At last some sky measurements were done to determine the receiver temperature and the atmospheric opacity. The receiver temperature was determined to be 110K - 150K depending on the LNB placing. Eventually, the atmospheric opacity at zenith was determined on an unstable cloudy day resulting in values of 0.039 and 0.053.

### 6.2 Further research

There are a lot of opportunities for further research using the single dish configuration or interferometer.

To determine the beam width of the single dish more accurately a 22 kHz tone could be added to use the High Frequency Band (HFB) of the LNB at 11.7 - 12.75 GHz. Using this band the FWHM for another frequency band can be determined and be compared with the theoretical value. The HFB could also be used to obtain parameters and compare them with the values found using the LFB.

As already mentioned in section 4.1.1, the found beam width of the main lobe only gives a lower bound. The measurement could be improved by isolating one specific satellite and by sweeping across the source from different sides instead of only vertical. The average of the found beam widths could be represented since it should be symmetrical. Besides, the beam width in the FF was only determined along the semi major axis of the dish which was shown to be less accurate according to the NF scans. The FF scan could be done over again mounting the dish on a  $90^\circ$  angle and sweeping across the source along the semi-minor axis of the dish, giving a more symmetrical (and accurate) result. Another option to determine the beam width more accurately could be by using an artificial point source on earth. It would be perfect to do this in a room particularly for this kind of measurements so that the sky and surroundings will not influence your results.

The beam width was determined by fitting a Gaussian profile through the main beam. At first, the Gaussian seems to give the optimal fit but other profiles such as a sinc or bessel function squared could also be fitted and be compared with the Gaussian.

For all the (single dish) measurements, the same dish and LNB were used. It would be interesting to compare the 2 dishes and 2 LNB's with each other to see if there are any (remarkable) differences. These potential differences are also interesting for the interferometer since it would cause inconsistencies.

In section 5.1 the receiver temperature was determined using an atmospheric model without calibration and by assuming the same gain to be the same as a few weeks before. This is not very accurate, since the LNB placing was really different resulting in a different gain. This measurement could be done over again using Y-factor calibration to get a better estimate of the receiver temperature and atmospheric opacity. This would require a larger cold load to be made so that the beam is completely filled.

Using attenuators, the output of a system could be compared to the input from which the linearity of the individual components could be mapped.

It was found that there is spillover from the illumination of the LNB onto the dish. The Y-factor calibration could be done using different LNB positions. In this way the spillover could be mapped as a function of LNB distance, making it easy to choose which Gain-to spillover ratio satisfies specific measuring conditions.

As stated in section 3.4, the sensitivity could be increased by extending the integration time. When using integration times of seconds, Astrophysical objects such as Cassiopeia A and Taurus A should be visible for the interferometer. Just as determining the angular size of the sun done by Farret Jentink (Farret Jentink, 2018), the same could be done for these objects.

Using the new tracking-devices, objects such as the sun or moon could be observed using longer integration times. Since the projection of the baseline changes, the fringe-speed changes as a function of time making it easier to obtain the visibility function.

At last the movement of geostationary satellites could be determined. Using the interferometer, the relative velocity of geostationary satellites emitting radiation at our observing frequency would cause differences in fringe speed. Using the distance ( $\approx 36.000\text{km}$ ) to the satellite and this difference, the deviation from the geosynchronous equatorial orbit of the satellite can be determined.



## Appendix A

# Python script for calibration and elevation scans

```

matplotlib inline
import numpy as np
import matplotlib.pyplot as plt
import matplotlib
import math

#P1,time1 = np.loadtxt('data_KISS/sun.txt'
, comments="#", unpack=True, usecols=(0,1))
time2,P2 = np.loadtxt('data_KISS/testload3.txt'
, comments="#", unpack=True, usecols=(0,1))
#P3,time3 = np.loadtxt('data_KISS/test3.txt'
, comments="#", unpack=True, usecols=(0,1))

#print(len(P2))
#print(len(time2))
#P2 = 10**((P2)/10)
time = 783*0.5
degree = (5*90)/6

fig = plt.figure(dpi=1200)
frame1 = fig.add_subplot(111)
fig.set_size_inches(15,10)
frame1.plot(time2,P2, label = 'Power_hot/cold_load')
#frame1.plot(np.linspace(15,70,100)
,np.linspace(0,0.00001,100)-3)
frame1.plot(P1,time1, label = '$B_{141cm}$')
frame1.plot(P2,time2, label = '$G_{bandpass}(j_{\omega})$')
frame1.plot(P3,time3, label = '$G_{bandpass}(j_{\omega})$')
frame1.set_xlabel('Time(s)',fontsize=24)
frame1.set_ylabel('Power(dBm)',fontsize=24)
frame1.set_xlim(0,700)
#frame1.set_ylim(0.0131,0.0134)
frame1.legend(loc=4,fontsize=26)
plt.tick_params(axis='both',labelsize=24,color='k')
frame1.grid(True)

Phot2=np.mean(10**((P2[1020:1120]/10)))
Pcold2=np.min(10**((P2[970:1010]/10)))

Phot1=np.mean(10**((P2[141:190]/10)))
Pcold1=np.min(10**((P2[301]/10)))
Thot1=24.2 +273.15
Thot2=24.1+273.15
Tcold= 77.15 #K
#print(Phot1,Phot2,Pcold1,Pcold2)
# 1 = only lnb, 2 = dish + lnb
Y1 = Phot1/Pcold1
Y2 = Phot2/Pcold2

Trx1=(Thot1-Tcold*Y1)/(Y1-1)
Trx2=(Thot2-Tcold*Y2)/(Y2-1)
print(Trx1,Trx2)

bw=10**9 # Hz
kb = 1.381*10**-23 #...
c = 3*10**8
v = 11.2*10**9
d= 0.35 #m
r = 0.5*d
lamb = c/v
Ae = np.pi*r**2
Gdish=(4*np.pi*Ae/(lamb**2))
print("gaindish",math.log10(Gdish)*10)
#((Phot1-Pcold1)/(kb*bw*(Thot1-Tcold)))
#print(((Phot2-Pcold2)/(kb*bw*(Thot2-Tcold))))
G2 = Pcold2/(Trx2+Tcold)

G1 = Pcold1/(Trx1+Tcold)
print(1/G1,1/G2)
#print(math.log10((Gdish/G1))*10)
#print(math.log10(1/G2)*10)
#print(G1,G2)
print(math.log10(Gdish)*10)

```

```

print(Phot2, Phot1)
#print(Gdish)
#print((1/G1)*Gdish)
print(10*math.log10(1/G2))

print(Pcold1, Pcold2)

time3, P = np.loadtxt('data_KISS/data234846_powermeasure.txt',
, comments="#", unpack=True, usecols=(0,1))
P = 10*(P/10)
P = P[230:330]*38000
time4 = time3[230:330]*1.8*97.5/251.5 - 80
import scipy.optimize as optimization
sigma1 = [0.3]*len(time4)

def func(x, a, b, c, d):
    return 25 + 273.15 + c + a*np.exp(b/np.cos(x+d))

params = optimization.curve_fit(func,
np.deg2rad(time4)
,P,p0=(-20,0.05,100,10)
,sigma=sigma1) #lsq fitting
a = params[0][0]
b = params[0][1]
c = params[0][2]
d = params[0][3]
berr = params[1][1][1]

print("a:", a)
print("b:", b)
print("c:", c)
print("d:", d)

fig = plt.figure(dpi=1200)
fig.set_size_inches(15, 10)
frame1 = fig.add_subplot(111)
frame1.plot(time4, P, label = 'Elevation_scan_1')
frame1.plot(time4, func(np.deg2rad(time4), a, b, c, d))
frame1.set_xlabel('Zenith_angle_$(^{\circ})$', fontsize=20)
plt.tick_params(axis='both', labelsize=18, color='k')
frame1.set_ylabel('Temperature_(K)', fontsize=20)
frame1.legend(fontsize=24, loc=2)
frame1.grid(True)

```

## Appendix B

# Python script for determining Allan variance

This code was obtained from Lap (Lap, [2015](#)) and modified for to fit our needsings.

```
import numpy as np
import matplotlib.pyplot as plt
import matplotlib

def sigma2(k, y):
# Allan Variance
    diffs = np.empty(0)
    for i in range(0, len(t)-k, k):
        value_i = y[i:i+k].mean()
        value_i_plus_one = y[i+k:i+2*k].mean()
        diff2 = (value_i - value_i_plus_one)**2 / 2
        diffs = np.append(diffs, diff2)
    return diffs.mean()

# Load data
t, y = np.loadtxt('data_KISS/stabilityhot1.txt', unpack=True)
y = 10**(y/10)

# Determine allan Variance
N = len(t) # Number of samples
thau_multipliers = np.array(range(1, int(N/2)))

# Allan Variance Plot
fig = plt.figure()
frame1 = fig.add_subplot(111)
frame1.loglog(thau_multipliers*0.05, [sigma2(k,y)
for k in thau_multipliers], label='40_min_measurement')
frame1.set_xlabel('$t_{s}$')
frame1.set_ylabel(r'$Allan_{Variance}_{\sigma_{y}^2}$')
frame1.set_title
('Allan_{Variance}_{plot}_{of}_{the}_{system}_{noise}')
frame1.set_ylim(10**-13, 10**-8)
frame1.legend()
frame1.grid(True)

# Show
plt.show()
"""

def sigma2(k, y):
# Allan Variance
    diffs = np.empty(0)
    for i in range(0, len(t)-k, k):
        value_i = y[i:i+k].mean()
        value_i_plus_one = y[i+k:i+2*k].mean()
        diff2 = (value_i - value_i_plus_one)**2 / 2
        diffs = np.append(diffs, diff2)
    return diffs.mean()

# Load data
t, y = np.loadtxt('data_KISS/stability2h.txt', unpack=True)
t = t[4000:7500]
y = y[4000:7500]
y1 = 10**(y/10)

# Determine allan Variance
N = len(t) # Number of samples
thau_multipliers1 = np.array(range(1, int(N/2)))

# Allan Variance Plot
fig = plt.figure()
frame1 = fig.add_subplot(111)
frame1.loglog(thau_multipliers1*0.05, [sigma2(k,y1)
for k in thau_multipliers1], label="2 Hour measurement")
frame1.set_xlabel('$t_{s}$')
frame1.set_ylabel(r'$Allan_{Variance}_{\sigma_{y}^2}$')
frame1.set_title
('Allan_{Variance}_{plot}_{of}_{the}_{system}_{noise}')
frame1.set_xlim(0.01, 1000)
```

```
frame1.set_ylim(10**-13,10**-8)
frame1.legend()
frame1.grid(True)

# Show
plt.show()
```

## Appendix C

# Python Script for determining beampattern using the FF-scan

```

import matplotlib.pyplot as plt
import matplotlib

time2,P2 = np.loadtxt('data_KISS/HPBW1.txt', comments="#",
, unpack=True, usecols=(0,1))
time1,P1 = np.loadtxt('data_KISS/HPBW2.txt', comments="#",
, unpack=True, usecols=(0,1))
time = 783*0.5
degree = (5*90)/6

P3 = 0.1*10**((P3)/10)
P3 = P3 - np.min(P3)
#P2 = 10**((P1-30)/10)
time = 783*0.5
degree = (5*90)/6

Baseline1 = 1410 #mm
Baseline2 = 2655 #mm
Baseline3 = 5130 #mm
ratio=77/(24*60)*360/time2[-1]
time2=ratio*time2
time1=ratio*time1

#P2 = 10**((P2)/10)
P2 = P2- np.max(P2)
P1 = 10**((P1)/10)
P1 = P1-np.min(P1)
time1 = np.arange(30,47,0.01)

fig = plt.figure(dpi=1200)
fig.set_size_inches(15, 10)
frame1 = fig.add_subplot(111)
frame1.plot((time2+30),-0.000017/17*(time2-20)
,label = '$line$')
frame1.plot(time2+30,P2[:: -1],label = '$satellite_{2}$')
#frame1.plot(time1+30,P1[:: -1],label = '$satellite_{1}$')
frame1.set_xlabel('$Elevation_{angle_{\circ}}$')
,fontsize=20)
frame1.set_ylabel('$power_{mW}$', fontsize=20)
#frame1.set_xlim(30,31)
#frame1.set_ylim(0,0.001)
frame1.legend(fontsize=24,loc=1)
frame1.grid(True)

import scipy.optimize as optimization

def func2(x, a, mu, sigma):
    return a*np.exp(-(x-mu)**2/(2*sigma**2))
i = 0
j = len(time2)
signal = [0.001]*(j-i)
params = optimization.curve_fit(func2, 30+time2[i:j]
, P2[i:j],p0=[0.00005,40,1],sigma=signal) #lsq fitting
a = params[0][0]
mu = params[0][1]
sigma = params[0][2]

berr = params[1][1][1]

print("mu:",mu)
print("sigma:", sigma)

#print("The WFM:",2.355*(sigma))
mu=11.2*10**9 # Hz
c = 299792458 #m/s
D = 0.352 # m
res = c /(mu*D)
#print('real_res=',res*180/np.pi)
Pnew = P2
max3 = np.max(Pnew[3700:4114])
max2 =np.max(Pnew)-0.1

```

```

max1=np.max(Pnew[500:1300])
print(max1,max2,max3)
min1=np.min(Pnew[1000:1300])
max1new=max1-min1
print(max1new)
print(30+time2[1000],30+time2[1300])
a= 30+8.1
fig = plt.figure(dpi=1200)
fig.set_size_inches(15,10)
frame1 = fig.add_subplot(111)
frame1.plot(30+time2-a,P2/, label = 'Satellite_1',color='g')
#plt.axhline(y=0.000031
, label = 'side_lobe_1_(31.2,0.000031)',color='r')
#plt.axhline(y=0.0070
, label = 'main_lobe_(38.1,0.0070)',color='b')
#plt.axhline(y=0.00013
, label='side_lobe_2_(45.1,0.00013)',color='y')
plt.axvline(x=31.2-a,color='b')
plt.axvline(x=38.1-a,color='b')
plt.axvline(x=45.1-a,color='b')
plt.axhline(y=-3,color='k')
plt.axhline(y=-3,color='k')
plt.axvline(x=38.1-a-2.7,color='k')
plt.axvline(x=38.1-a+2.4,color='k',label='-3dB_line')
plt.axvline(x=38.1-a+4.12,color='r',lw=3,ls=":")
plt.axvline(x=45.1-a-11.12,color='r',lw=3,ls=":")
plt.axhline(y=-6,label='symmetrical_lines',color='r',
lw=3,ls=":")
plt.tick_params(axis='both',labelsize=18,color='k')
plt.xticks(np.arange(-10, 10, 1))
#frame1.plot(30+time2,func2(30+time2,a,mu,sigma),
label = 'Gaussian_fit_FWHM_-'
+ str(round(2.355*(sigma), 2)) + '$^{\circ}$'
,color='orange',lw=2)
frame1.set_xlabel('Elevation_angle_$(^{\circ})$', fontsize=20)
frame1.set_xlim(-8.1,9)
#frame1.set_ylim(0.00,0.00005)
frame1.set_ylabel('Power_(dBm)', fontsize=20)
frame1.legend(fontsize=18,loc=1)
frame1.grid(True)

```

## Appendix D

# Python Script for determining beampattern using the $NF_1$ -scan

This code was obtained from Lap (Lap, [2015](#)) and modified for to fit our needsings.

```
#!/usr/bin/env python
# -*- coding: utf-8 -*-
import math
import numpy as np
from matplotlib.pyplot import *
from mpl_toolkits.mplot3d import Axes3D

x1, y1, z1, real1, imaginary1
= np.loadtxt('lnbscanlambda.txt', usecols=(0,1,2,5,6),
unpack=True)
x2, y2, z2, real2, imaginary2
= np.loadtxt('lnbscan.txt', usecols=(0,1,2,5,6),
unpack=True)
da=50
Nz = da
Ny = da
print(len(x1),len(y1),len(real1))
def sort_by_freq(re, im, Ny, Nz, freq_element):
    freq = np.linspace(10,12,21)
    #print "Matrix will be calculated for "
    + str(freq[freq_element])+ " GHz"
    matrix = np.zeros((Nz,Ny),dtype=complex)
    real_sorted = []
    imaginary_sorted = []

    k = freq_element
    p = freq_element

    while k < len(re):
        real_sorted.append(re[k])
        k += 21

    while p < len(im):
        imaginary_sorted.append(im[p])
        p += 21

    h = 0
    for i in range(Nz):
        for j in range(Ny):
            matrix[i][j] = real_sorted[h]
            + imaginary_sorted[h]*1j
            h += 1

    return matrix

def intersect(value, x, y):
    '''Find the x left coordinate corresponding to
    value assuming a symmetric function w.r.t.x.
    Intersect fits a straight line through the points
    just above and just below the wanted value and then
    interpolates the wanted number.
    '''
    N = len(y)
    # Go halfway
    for i in range(N/2 + 1):
        if y[i] > value:
            y_low = y[i-1]
            y_high = y[i]
            x_low = x[i-1]
            x_high = x[i]
            break
    # Linear interpolation.
    slope = (y_high - y_low) / (x_high - x_low)
    x = (value - y_low) / slope + x_low
    return x

def fieldplots(real1, imaginary1, real2, imaginary2,
Ny, Nz, selected): #Calculate the field plots.
    A1 = np.zeros((Nz,Ny),dtype=complex)
    A2 = np.zeros((Nz,Ny),dtype=complex)
    frequencies = np.arange(11.2,11.3,0.1)
    A1_fft_sum = 0
```

```

lowerfreq = np.round(selected[0], decimals=1)
higherfreq = np.round(selected[len(selected)-1],
, decimals=1)

for t in range(len(selected)):
    A = sort_by_freq(real1,imaginary1,da
,da,selected[t])
    B = sort_by_freq(real2,imaginary2,da
,da,selected[t])

    A1 += (A + 1j*B)/2

# Nearfield
A1_near_amp = abs(A1)
A1_near_phase = np.arctan2(np.imag(A1),np.real(A1))

theta = np.linspace(-14,14,da)
maximum = 0
for i in range(Nz):
    for j in range(Ny):
        if A1_near_amp[i][j] > maximum:
            maximum = A1_near_amp[i][j]
            index_z = i
            index_y = j
A1_near_amp_T = A1_near_amp.T

# For one frequency
if lowerfreq == higherfreq:
    fig1 = plt.figure()
    fig1.set_size_inches(15, 10)
    ax = fig1.add_subplot(111)
    ax.set_xlabel('y_(cm)', fontsize=28)
    ax.set_ylabel('z_(cm)', fontsize=28)
    #ax.set_xticks(np.linspace(-14,14,9))
    #ax.set_yticks(np.linspace(-14,14,9))
    ax.tick_params(axis='both', which='major'
, labelsz=28)
    ax.set_title('Amplitude_near-field_for_' +
str(np.round(lowerfreq, decimals=0)) + '_GHz'
, fontsize=28)
    cax = ax.imshow(10*np.log10((A1_near_amp
/np.amax(A1_near_amp)))**2)
    ,vmin=-40,vmax=0,extent=[-14,14,-14,14])
    cbar = fig1.colorbar(cax)
    cbar.set_label('Power_(dB)', fontsize=28)
    a = str(lowerfreq)
    b = ""
    for c in a:
        if c != ".":
            b += c
        else:
            b += ","
    savefig('Nearfield_amplitude_' + b
+ '_GHz.png')
    show()

    fig1 = plt.figure()
    fig1.set_size_inches(15, 10)
    ax = fig1.add_subplot(111)
    x = np.linspace(-40,40,da)
    plot(x,10*np.log10((A1_near_amp[index_z]
/np.amax(A1_near_amp[index_z]))**2)
, label='maximum_along_z', linewidth=2)
    plot(x,10*np.log10((A1_near_amp_T[index_y]
/np.amax(A1_near_amp_T[index_y]))**2)
, label='maximum_along_y', linewidth=2)
    title('Maximum_amplitude_crosscut
near-field_for_'
+ str(np.round(lowerfreq, decimals=0))
+ '_GHz', fontsize=28)
    ax.set_xticks(np.linspace(-14,14,5))
    ax.tick_params(axis='both', which='major'
, labelsz=28)
    xlabel("distance from center (cm)"
, fontsize=28)
    ylabel("Power (dB)", fontsize=28)
    legend(loc='lower_center')
    savefig('Nearfield_amplitude_crosscut_'
+b+ '_GHz.png')
    show()

    fig1 = plt.figure()
    fig1.set_size_inches(15, 10)
    ax = fig1.add_subplot(111)
    ax.set_xlabel('y_(cm)', fontsize=20)
    ax.set_ylabel('z_(cm)', fontsize=20)
    ax.tick_params(axis='both', which='major'
, labelsz=28)
    ax.set_title('Phase_near-field_for_'
+ str(np.round(lowerfreq, decimals=0))
+ '_GHz', fontsize=28)
    cax = ax.imshow(A1_near_phase
, extent=[-14,14,-14,14])
    # fig1.colorbar(cax)

    savefig('Nearfield_phase_'

```



```

        +b+'_GHz.png')
        show()

# For multiple frequencies
else:
    a = str(lowerfreq)
    b = ""
    for c in a:
        if c != ".":
            b += c
        else:
            b += ","

    a = str(higherfreq)
    d = ""
    for e in a:
        if e != ".":
            d += e
        else:
            d += ","

    fig1 = plt.figure()
    fig1.set_size_inches(15, 10)
    ax = fig1.add_subplot(111)
    ax.set_xlabel('yz(cm)', fontsize=20)
    ax.set_ylabel('zz(cm)', fontsize=20)
    ax.set_title('Amplitude_nearfield_for_'
        + str(lowerfreq)
        + '-' + str(higherfreq) + '_GHz', fontsize=24)
    cax = ax.imshow(10*np.log10((A1_near_amp
        /np.amax((A1_near_amp)))**2)
        ,vmin=-40,vmax=0,extent=[-14,14,-14,14])
    fig1.colorbar(cax)
    cax.set_label("Power (dB)")
    savefig('Nearfield_amplitude_' + b + '-'
        + d + '_GHz.png')
    show()

    fig1 = plt.figure()
    fig1.set_size_inches(15, 10)
    ax = fig1.add_subplot(111)
    x = np.linspace(-40,40,da)
    plot(x,10*np.log10((A1_near_amp[index_z]
        /np.amax(A1_near_amp[index_z]))**2)
        , label='maximum_along_z',linewidth=2)
    plot(x,10*np.log10((A1_near_amp_T[index_y]
        /np.amax(A1_near_amp_T[index_y]))**2)
        ,label='maximum_along_y',linewidth=2)
    title('Maximum_amplitude_cross_cut
        nearfield_for_'
        + str(lowerfreq) + '-' + str(higherfreq)
        + '_GHz', fontsize=24)
    xticks(np.linspace(-14,14,5))
    xlabel('distance_from_center_(cm)'
        ,fontsize=20)
    ylabel('Power_(dB)', fontsize=20)
    legend(loc='lower_center')
    savefig('Nearfield_amplitude_crosscut_'
        + b + '-' + d + '_GHz.png')
    show()

    fig1 = plt.figure()
    fig1.set_size_inches(15, 10)
    ax = fig1.add_subplot(111)
    ax.set_xlabel('yz(cm)', fontsize=20)
    ax.set_ylabel('zz(cm)', fontsize=20)
    ax.set_title('Phase_nearfield_for_'
        + str(lowerfreq)
        + '-' + str(higherfreq) + '_GHz', fontsize=24)
    cax = ax.imshow(A1_near_phase
        ,extent=[-14,14,-14,14])
    fig1.colorbar(cax)

    savefig('Nearfield_phase' + b + '-' + d + '_GHz.png')
    show()

# Farfield
c = 29979245800 #cm/s
f = 11.25e9
unit = 280
lambda_0 = c/f #mm
D= 15
element_number1 = np.arange(1,25,1)
*(lambda_0*D/unit)
#Hier moet jij van maken: np.arange(1,41,1)
*(lambda_0*D/400)
waarbij de D de afstand tot de spiegel is
element_number2 = -1*np.arange(25,0,-1)
*(lambda_0*D/unit)
# Hetzelfde hier als in regel 295
zero = np.array(0)
x = np.hstack((element_number2, zero ,element_number1))

theta_y = np.degrees(np.arctan(x))
theta_z = np.degrees(np.arctan(x))
print(len(theta_z))
A1_far_amp = abs(np.fft.fftsift(np.fft.fft(A1)))
A1_far_phase = np.arctan2(np.imag(A1),np.real(A1))

```

```

theta = np.linspace(-14,14,da)
maximum = 0
for i in range(Nz):
    for j in range(Ny):
        if A1_far_amp[i][j] > maximum:
            maximum = A1_far_amp[i][j]
            index_z = i
            index_y = j
A1_far_amp_T = A1_far_amp.T

y = 10*np.log10((A1_far_amp[index_z]/
np.amax(A1_far_amp[index_z]))**2)
z = 10*np.log10((A1_far_amp_T[index_y]/
np.amax(A1_far_amp_T[index_y]))**2)

# For one frequency
if lowerfreq == higherfreq:
    a = str(lowerfreq)
    b = ""
    for c in a:
        if c != ".":
            b += c
        else:
            b += ","

    fig2 = plt.figure()
    fig2.set_size_inches(15, 10)
    ax = fig2.add_subplot(111)
    ax.set_xlabel('y-angle_($^\circ$)',
, fontsize=20)
    ax.set_ylabel('z-angle_($^\circ$)',
, fontsize=20)
    ax.set_xticks(np.linspace(-70,70,15))
    ax.set_yticks(np.linspace(-70,70,15))
    ax.set_title('Amplitude_far-field_'
+ str(np.round(lowerfreq, decimals=0))
+ '_GHz', fontsize=24)
    cax = ax.imshow(10*np.log10((A1_far_amp
/np.amax(A1_far_amp)))**2)
, vmin=-40, vmax=0, extent=[-70,70,-70,70])
    cbar=fig2.colorbar(cax)

    cbar.set_label('Power_(dB)', size=20)
    savefig('Farfield_amplitude_' + b + '_GHz.png')
    show()

    ax = fig2.add_subplot(122)
    #x = np.linspace(-40,40,81)
    plot(theta_z, z, label='maximum_along_y',
, linewidth=2)
    plot(theta_y, y, label='maximum_along_z',
, linewidth=2)
    title('Maximum_amplitude_cross_cut_far-field_'
+ str(np.round(lowerfreq, decimals=0))
+ '_GHz', fontsize=24)
    legend(loc='lower_center')
    xlim([-70,70])
    #xticks(np.linspace(-40,40,9))
    xlabel('Angle_($^\circ$)', fontsize=20)
    ylabel('Power_(dB)', fontsize=20)
    savefig('Farfield_amplitude_crosscut_'
+ b + '_GHz.png')
    show()

# For more than one frequency
else:
    a = str(lowerfreq)
    b = ""
    for c in a:
        if c != ".":
            b += c
        else:
            b += ","

    a = str(higherfreq)
    d = ""
    for e in a:
        if e != ".":
            d += e
        else:
            d += ","

    fig2 = plt.figure()
    fig2.set_size_inches(15, 10)
    ax = fig2.add_subplot(121)
    ax.set_xlabel('y_(cm)', fontsize=20)
    ax.set_ylabel('z_(cm)', fontsize=20)
    ax.set_title('Amplitude_farfield_'
+ str(lowerfreq)
+ '-' + str(higherfreq) + '_GHz'
, fontsize=24)
    cax = ax.imshow(10*np.log10((A1_far_amp
/np.amax(A1_far_amp)))**2)
, vmin=-40, vmax=0)
    fig2.colorbar(cax)
    cax.set_label("Power (dB)")
    savefig('Farfield_amplitude_' + b + '-' +

```

```

+d+ '_GHz.png')
show()

ax = fig2.add_subplot(122)
x = np.linspace(-14,14,da)
plot(x,z, label='maximum_along_y',
      ,linewidth=2)
plot(x,y, label='maximum_along_z',
      ,linewidth=2)
title('Maximum amplitude
cross_cut_nearfield_
+ str(lowerfreq) + '_
+ str(higherfreq)
+ '_GHz', fontsize=24)
legend(loc='lower_center')
xticks(np.linspace(-40,40,9))
xlabel('distance_from_center_cm')
, fontsize=20)
ylabel('Power_dB', fontsize=20)
savefig('Farfield_amplitude_crosscut_
+b+ '-d+ '_GHz.png')
show()

return z, y, lowerfreq, higherfreq

def beamsize(z,y, Ny, Nz, lowerfreq, higherfreq):
# bepalen van de beamsize
c = 29979245800 #cm/s
f = 11.25e9
unit = 280
lambda_0 = c/f
D = 15 #
element_number1 = np.arange(1,25,1)
*(lambda_0*D/unit)
#Hier moet jij van maken: np.arange(1,41,1)
*(lambda_0*D/400)
waarbij de D de afstand tot de spiegel is
element_number2 = -1*np.arange(25,0,-1)
*(lambda_0*D/unit)
# Hetzelfde hier als in regel 295
zero = np.array(0)
x = np.hstack((element_number2, zero, element_number1))

theta_y = np.degrees(np.arctan(x))
theta_z = np.degrees(np.arctan(x))

# along y-axis
y_min_beamsize = intersect(-3, theta_y, y)
y_min_beamsize_rad = np.radians(y_min_beamsize)
# Half angle in radians
y_min_beamsize_deg = y_min_beamsize
# Half angle in degrees

y_max_beamsize = intersect(-3,-1*theta_y,y)
y_max_beamsize_rad = np.radians(y_max_beamsize)
# Half angle in radians
y_max_beamsize_deg = y_max_beamsize
# Half angle in degrees

y_beamsize_avg_deg =
(abs(y_min_beamsize_deg)+abs(y_max_beamsize_deg))/2
y_beamsize_avg_rad =
(abs(y_min_beamsize_rad)+abs(y_max_beamsize_rad))/2

print(' Beamsize_(full_angle)_along_z-axis:_'
, np.round((2*y_beamsize_avg_deg),decimals=2)
, '_degrees')
print('Beam_solid_angle_along_z-axis:_'
, (y_beamsize_avg_rad**2)*np.pi, '_steradian')

# along z-axis
z_min_beamsize = intersect(-3, theta_z, z)
z_min_beamsize_rad = np.radians(z_min_beamsize)
# Half angle in radians
z_min_beamsize_deg = z_min_beamsize
# Half angle in degrees

z_max_beamsize = intersect(-3,-1*theta_z,z)
z_max_beamsize_rad = np.radians(z_max_beamsize)
# Half angle in radians
z_max_beamsize_deg = z_max_beamsize
# Half angle in degrees

z_beamsize_avg_deg = (abs(z_min_beamsize_deg)
+abs(z_max_beamsize_deg))/2
z_beamsize_avg_rad = (abs(z_min_beamsize_rad)
+abs(z_max_beamsize_rad))/2

print(' Beamsize_(full_angle)_along_y-axis:_'
, np.round((2*z_beamsize_avg_deg)
,decimals=2)
, '_degrees')
print('Beam_solid_angle_along_y-axis:_'
, (z_beamsize_avg_rad**2)*np.pi, '_steradian')
print('Average_beam_size_',
(y_beamsize_avg_deg+z_beamsize_avg_deg)

```

```

, '_degrees')

#one frequency

if lowerfreq == higherfreq:
    a = str(lowerfreq)
    b = ""
    for c in a:
        if c != ".":
            b += c
        else:
            b += ","

#x, k = np.loadtxt('final_beampattern.txt'
, usecols=(0,1), unpack=True)
#k_real = 10**(k/10)
#k_real_norm = k_real/np.amax(k_real)
#k_db_norm = 10*np.log10(k_real_norm)

#beamsize_x = intersect(-3,x,k_db_norm)
#k_size = beamsize_x*-2

#y_min = y_min_beamsize_deg
#y_max = y_max_beamsize_deg

fig3 = plt.figure()
fig3.set_size_inches(15, 10)

ax = fig3.add_subplot(121)
ax.plot(theta_y, y, 'b',
label="Measured_data\nBeamwidth:"
+str(np.round((2*y_beamsize_avg_deg
, decimals=2))+"$^\circ$'
, linewidth=2)
# ax.vlines(y_min, 0, 'r'
, label='Beamsize:'
+str(np.round((2*y_beamsize_avg_deg
, decimals=2))
+'$^\circ$' , linewidth=2)
# ax.vlines(y_max, -80, 0, 'r' , linewidth=2)
#ax.vlines(4.4, -60, 0, 'k' ,
label='Theoretical: 8.8$^\circ$'
#ax.vlines(-4.4, -60, 0, 'k')
# ax.hlines(-3, -100, 100, 'g'
, label="-3 dB line"
, linewidth=2)
ax.set_xticks(np.linspace(-140, 140, 11))
ax.xaxis.set_minor_locator
(MultipleLocator(5))
ax.set_xlim([-70, 70])
ax.set_xlabel('Angle_\u($^\circ$)' , fontsize=20)
ax.set_ylabel('Power_\u(dB)'
, fontsize=20)
ax.set_title('Beam_pattern_horizontal_cut
+ str(np.round(lowerfreq
, decimals=0))
+'_GHz)'
, fontsize=20)
legend(loc='lower_center')

#z_min = z_min_beamsize_deg
#z_max = z_max_beamsize_deg

ax = fig3.add_subplot(122)
#ax.plot(x, k_db_norm, 'g', label="Simulated
data\nBeamwidth:" + str(np.round(k_size
, decimals=2))
+'$^\circ$' , linewidth=2)
# ax.hlines(-3, -180, 180, 'g'
, label="-3_dB_line"
, linewidth=2)
# ax.vlines(beamsize_x, 0, 0, 'k'
, label="Beamwidth: "
+str(np.round(k_size, decimals=2))+"$^\circ$"
, linewidth=2)
# ax.vlines(-1*beamsize_x,
0, 'k' , linewidth=2)
ax.set_ylim([-75, 0])

ax.plot(theta_z, z
, label='Measured_data\nBeamsize:'
+str(np.round((2*z_beamsize_avg_deg
, decimals=2))
+'$^\circ$' , linewidth=2)
# ax.vlines(z_min, -80, 0, 'r'
, label='Beamsize:'
+str(np.round((2*z_beamsize_avg_deg
, decimals=2))
+'$^\circ$' , linewidth=2)
# ax.vlines(z_max, -80, 0, 'r' , linewidth=2)
#ax.vlines(4.4, -60, 0, 'k'
, label='Theoretical: 8.8$^\circ$'
#ax.vlines(-4.4, -60, 0, 'k')
#ax.vlines(-38, -60, 0, 'y'
, label='Beam: 74$^\circ$'
#ax.vlines(36, -60, 0, 'y')
ax.set_xlim([-70, 70])

```

```

# ax.hlines(-3,-100,100,'g'
,label="-3 dB line",linewidth=2)
ax.set_xticks(np.linspace(-140,140,11))
ax.xaxis.set_minor_locator
(MultipleLocator(5))
ax.set_xlabel('Anglez($^\circ$)',
,fontsize=20)
ax.set_ylabel('Power(dB)',fontsize=20)
ax.set_title('Beampatternverticalcut
'+ str(np.round(lowerfreq,decimals=0))
+'GHz',fontsize=20)
legend(loc='lower_center')

tight_layout()

savefig('Beamsize_' + b + '_GHz.png')
show()

else:
    a = str(lowerfreq)
    b = ""
    for c in a:
        if c != ".":
            b += c
        else:
            b += ","

    a = str(higherfreq)
    d = ""
    for e in a:
        if e != ".":
            d += e
        else:
            d += ","

    y_min = y_min_beamsize_deg
    y_max = y_max_beamsize_deg
    fig3 = plt.figure()
    fig3.set_size_inches(15, 10)
    ax = fig3.add_subplot(121)
    ax.plot(theta_y,y, 'b', label='beamsize:
+str(np.round((2*y_beamsize_avg_deg)
,decimals=2))+ '$^\circ$')
    #ax.vlines(y_min,-60,0, 'r', label='Script')
    #ax.vlines(y_max,-60,0, 'r')
    #ax.vlines(4.4,-60,0, 'k',
    label='Theoretical: 8.8$^\circ$')
    ax.vlines(-45.2,-60,0, 'k')
    ax.vlines(41.8,-60,0, 'k')
    ax.hlines(-3,-160,160,'g'
,label='_3_dB_line')
    ax.hlines(-10,-160,160,'k'
,label='_10_dB_lines')
    ax.set_xticks(np.linspace
(-140,140,21))
    ax.xaxis.set_minor_locator
(MultipleLocator(5))
    ax.set_xlabel('Anglez($^\circ$)', fontsize=20)
    ax.set_ylabel('Power(dB)'
,fontsize=20)
    ax.set_ylim([-50,0])
    ax.set_xlim([-70,70])
    ax.set_title
('Beampatternseenalongz-axis_max._amp1_'
+ str(lowerfreq) + '_
+ str(higherfreq) + '_GHz')
    legend()

    z_min = z_min_beamsize_deg
    z_max = z_max_beamsize_deg
    ax = fig3.add_subplot(122)
    ax.plot(theta_z,z,label='beamsize:
+str(np.round((2*z_beamsize_avg_deg)
,decimals=2))
+' '$^\circ$')
    #ax.vlines(z_min,-60,0, 'r'
, label='Script')
    #ax.vlines(z_max,-60,0, 'r')
    #ax.vlines(4.4,-60,0, 'k',
    label='Theoretical: 8.8$^\circ$')
    #ax.vlines(-4.4,-60,0, 'k')
    #ax.vlines(-38,-60,0, 'y',
    label='Beam: 74$^\circ$')
    #ax.vlines(36,-60,0, 'y')
    ax.vlines(-47,-60,0, 'k')
    ax.vlines(42.5,-60,0, 'k')
    ax.hlines(-3,-160,160,'g'
,label='_3_dB_line')
    ax.hlines(-10,-160,160,'k'
,label='_10_dB_lines')
    #ax.xaxis.set_major_locator()
    ax.set_xticks(np.linspace(-140,140,21))
    ax.xaxis.set_minor_locator
(MultipleLocator(5))
    ax.set_xlabel('Angley($^\circ$)'
,fontsize=20)
    ax.set_ylabel('Power(dB)',fontsize=20)
    ax.set_ylim([-50,0])

```

```

        ax.set_xlim([-70,70])
        ax.set_title
        ('Beam_pattern_seen_along_y-axis_max.
        =====amp1_'+ str(lowerfreq) + '-'
        + str(higherfreq) + '_GHz')
        legend()

        tight_layout()

        savefig('Beamsize_'+b + '-' + d+'_GHz.png')
        show()

def resonance(real1, imaginary1, real2,
imaginary2, Ny, Nz, selected):
    A1 = np.zeros((Nz,Ny),dtype=complex)
    A2 = np.zeros((Nz,Ny),dtype=complex)
    freq = np.arange(10.5,11.6,0.1)
    A1_fft_sum = 0
    lowerfreq = np.round(selected[0]
    , decimals=1)
    higherfreq = np.round(selected[len(selected)-1]
    , decimals=1)

    for t in range(len(selected)):
        A = sort_by_freq(real1,imaginary1
        ,da,da,selected[t])
        B = sort_by_freq(real2,imaginary2
        ,da,da,selected[t])

        A1 += (A - 1j*B)/2

    # Nearfield
    A1_near_amp = abs(A1)
    A1_near_phase = np.arctan2(np.imag(A1)
    ,np.real(A1))

    fig1 = plt.figure()
    fig1.set_size_inches(15, 10)
    ax = fig1.add_subplot(111)
    ax.set_xlabel('y_(mm)')
    ax.set_ylabel('z_(mm)')
    ax.set_title('Standing_wave_nearfield_for_'
    + str(lowerfreq) + '-' + str(higherfreq) + '_GHz')
    cax = ax.imshow(10*np.log10((A1_near_amp
    /np.amax((A1_near_amp)))*2),vmin=-40,vmax=0)
    fig1.colorbar(cax)
    savefig('Standing_wave_horn_'+str(lowerfreq)
    + '-' + str(higherfreq) + '_GHz.png')
    show()

selected = np.arange(11.2,11.3,.1)
field = fieldplots(real1, imaginary1,
real1, imaginary1, Ny, Nz, selected)
z = field[0]
y = field[1]
lowerfreq = field[2]
higherfreq = field[3]

beamsize(z,y, Ny, Nz, lowerfreq, higherfreq)
resonance(real1, imaginary1, real2, imaginary2
, Ny, Nz, selected)

```

# Bibliography

- Balanis, Constantine A. (1982). "Antenna Theory, Analysis and Design". In: *John Wiley & Sons, Inc.* 2.
- Farret Jentink, Casper (2018). "Constructing the backend of the Kapteyn Interferometer for Short-Baseline Solar Observations (KISS)". In:
- Formsma, Job (2017). "Improving the Kapteyn Radio Telescope". In: URL: <https://www.astro.rug.nl/~formsma/JobFormsmaThesisFinal.pdf>.
- IEEE (2003). "521-2002 - IEEE Standard Letter Designations for Radar-Frequency Bands". In: URL: <https://ieeexplore.ieee.org/document/1160089/>.
- Lap, Bram (2015). "Design of a Pickett-Potter Horn to measure the CMB at 11 GHz". In: URL: [https://www.astro.rug.nl/opleidingsinstituut/reports/bachelor/Astro\\_Bc\\_2015\\_BNRLap.pdf](https://www.astro.rug.nl/opleidingsinstituut/reports/bachelor/Astro_Bc_2015_BNRLap.pdf).
- Lehpamer, Harvey (2010). "Microwave transmission networks: Planning, Design, and Deployment. USA: McGraw Hill Professional". In: 268–272.
- Loudon, R. (2000). "The Quantum Theory of Light". In: 3.
- M. Uhm, A. Shishlov and K. Park (1996). "Offset-paraboloid geometry: Relations for practical use". In: *IEEE Antennas Propag. Mag.* 38.3. URL: <http://www.john-legon.co.uk/offsetdish.htm>.
- Minoli, Daniel (2009). "Satellite Systems Engineering in an IPv6 Environment." In: USA: CRC Press.
- Mulder, Willeke (2015). "Calibration of a 11 GHz Pickett-Potter Horn". In: URL: [https://www.astro.rug.nl/opleidingsinstituut/reports/bachelor/Astro\\_Bc\\_2015\\_WMulder.pdf](https://www.astro.rug.nl/opleidingsinstituut/reports/bachelor/Astro_Bc_2015_WMulder.pdf).
- NCRA-TIFR (2002). "Aperture Efficiency". In: URL: [http://www.gmrt.ncra.tifr.res.in/gmrt\\_hpage/Users/doc/WEBLF/LFRA/node172.html](http://www.gmrt.ncra.tifr.res.in/gmrt_hpage/Users/doc/WEBLF/LFRA/node172.html).
- Rensburg, Juan-Pierre Jansen van (2012). "The design of a two-element correlation interferometer operating at L-band". In:
- Steringa, Jasper (2018). "Simulating the Visibilities of the Kapteyn Interferometer for Short Baseline Solar observations (KISS)". In:
- Sweijen, Frits (2015). "Computer Control of a Horn Antenna and Measuring the Sun at 11 GH". In: URL: [https://www.astro.rug.nl/opleidingsinstituut/reports/bachelor/Astro\\_Bc\\_2015\\_FSweijen.pdf](https://www.astro.rug.nl/opleidingsinstituut/reports/bachelor/Astro_Bc_2015_FSweijen.pdf).
- Wilson, Thomas L., Kristen Rohlf, and Susanne Hüttemeister (2013). "Tools of radio astronomy sixth edition". In:
- Woerden, Hugo van and Richard G. Strom (2006). "The beginnings of radio astronomy in the Netherlands". In: *Journal of Astronomical History and Heritage (ISSN 1440-2807)*. 9.1.
- Zandvliet, Maik (2015). "Back-end and Mechanics of a Pickett-Potter Horn Telescope at 11GHz". In: URL: [https://www.astro.rug.nl/opleidingsinstituut/reports/bachelor/Astro\\_Bc\\_2015\\_MZandvliet.pdf](https://www.astro.rug.nl/opleidingsinstituut/reports/bachelor/Astro_Bc_2015_MZandvliet.pdf).